

Calibration and Energy Scale in KamLAND

Azusa Gando for the KamLAND Collaboration
RCNS, Tohoku University

Contents

Detector

Overview of recent result

Energy reconstruction and calibration

Summary

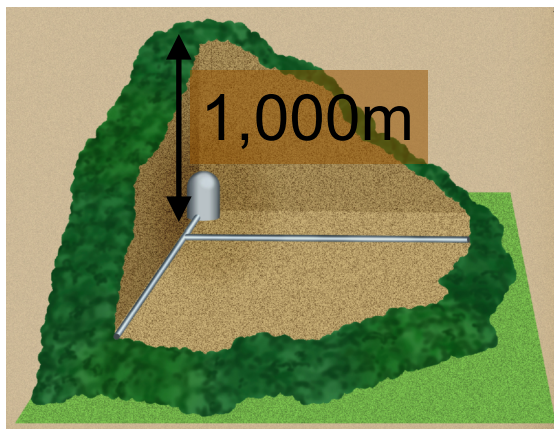
Detector

KamLAND Kamioka Liquid scintillator Anti Neutrino Detector

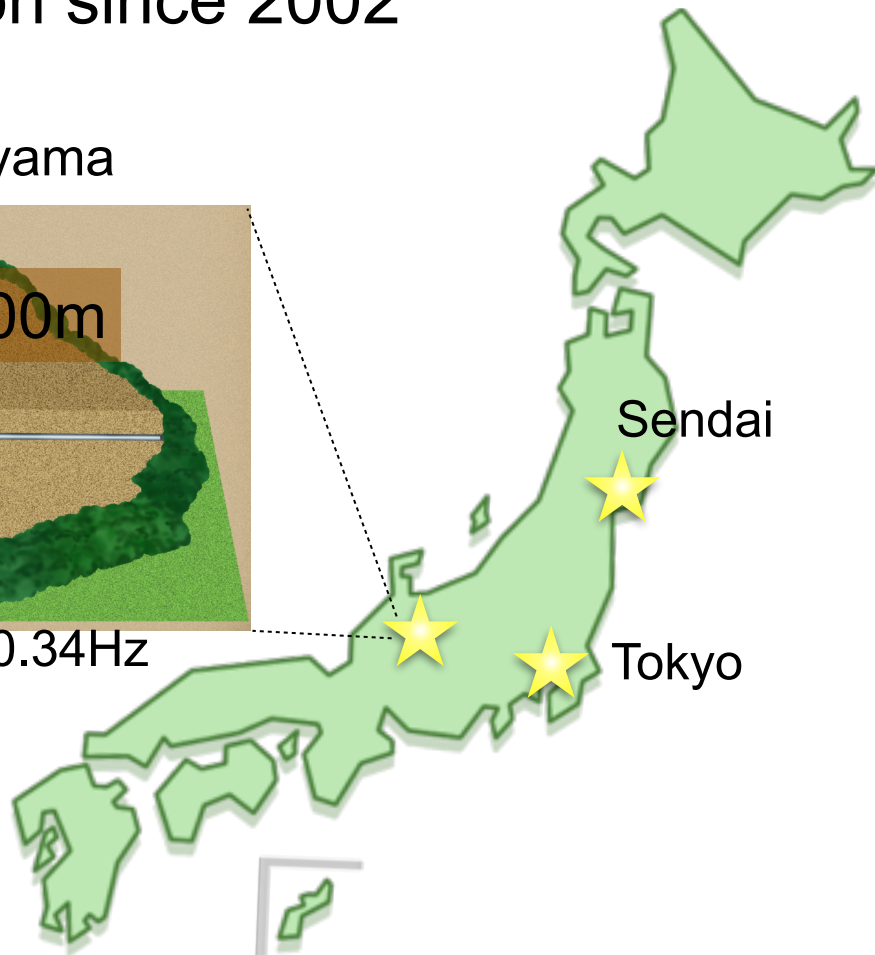
Located at Kamioka mine, Japan. ~2700 m.w.e.

In operation since 2002

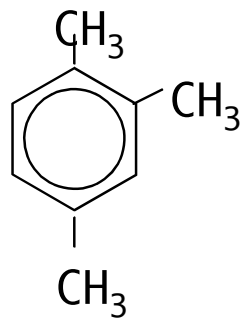
Mt. Ikenoyama



μ rate ~ 0.34Hz



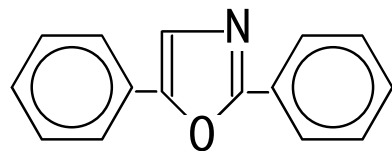
PC 20%



Dodecane 80%



PPO 1.36g/l



^{238}U : 3.5×10^{-18} , ^{232}Th : 5.2×10^{-17} [g/g]

Outer detector
(3,000 ton of water)

Buffer oil
1,800m³

Liquid scintillator
1000 ton
in R=6.5m balloon

20 inch PMT × 225
for outer detector

17 inch PMT × 1325
20 inch PMT × 554
Photo coverage 34%

20 m

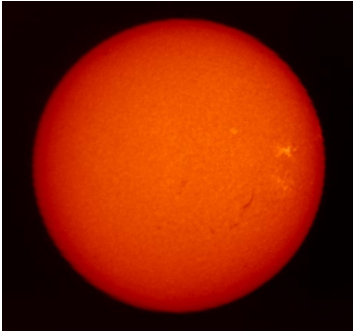
20 m

Physics target & Detection method



Electron scattering
 $\nu + e^- \rightarrow \nu + e^-$

^7Be solar neutrino



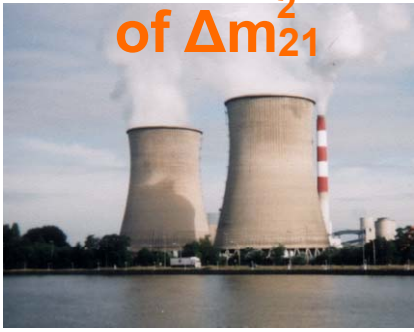
Neutrino
Astrophysics

Geo-neutrino
First detection!



Neutrino
Geophysics

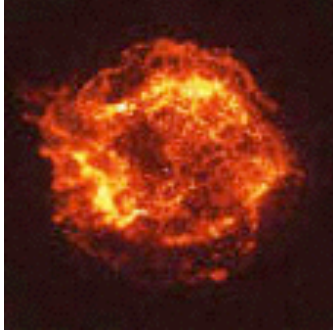
Reactor neutrino
**Precise measurement
of Δm_{21}^2**



Neutrino Physics

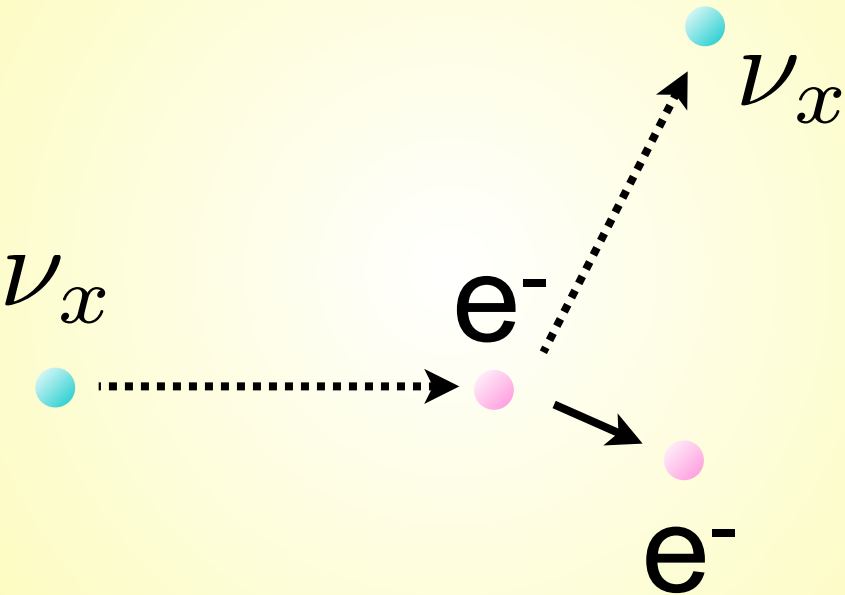
$\bar{\nu}_e + p \rightarrow e^+ + n$
Inverse beta decay

Supernova (relic) neutrino
GRB neutrino etc.

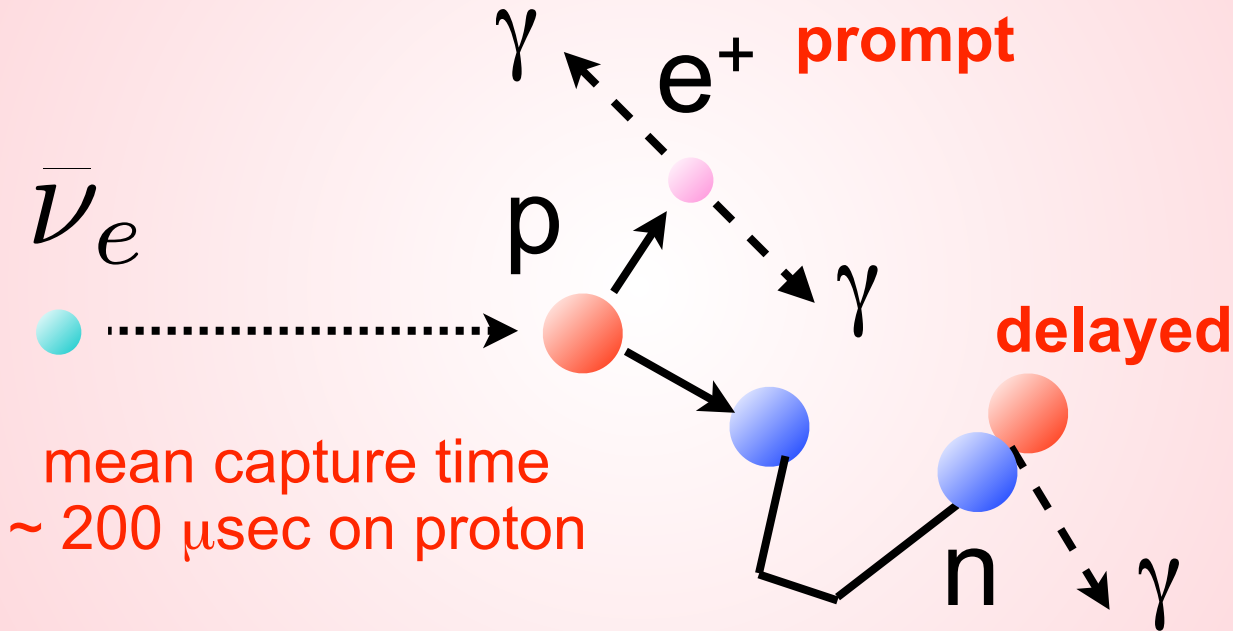


Neutrino Astrophysics
Cosmology

Electron scattering → Single event



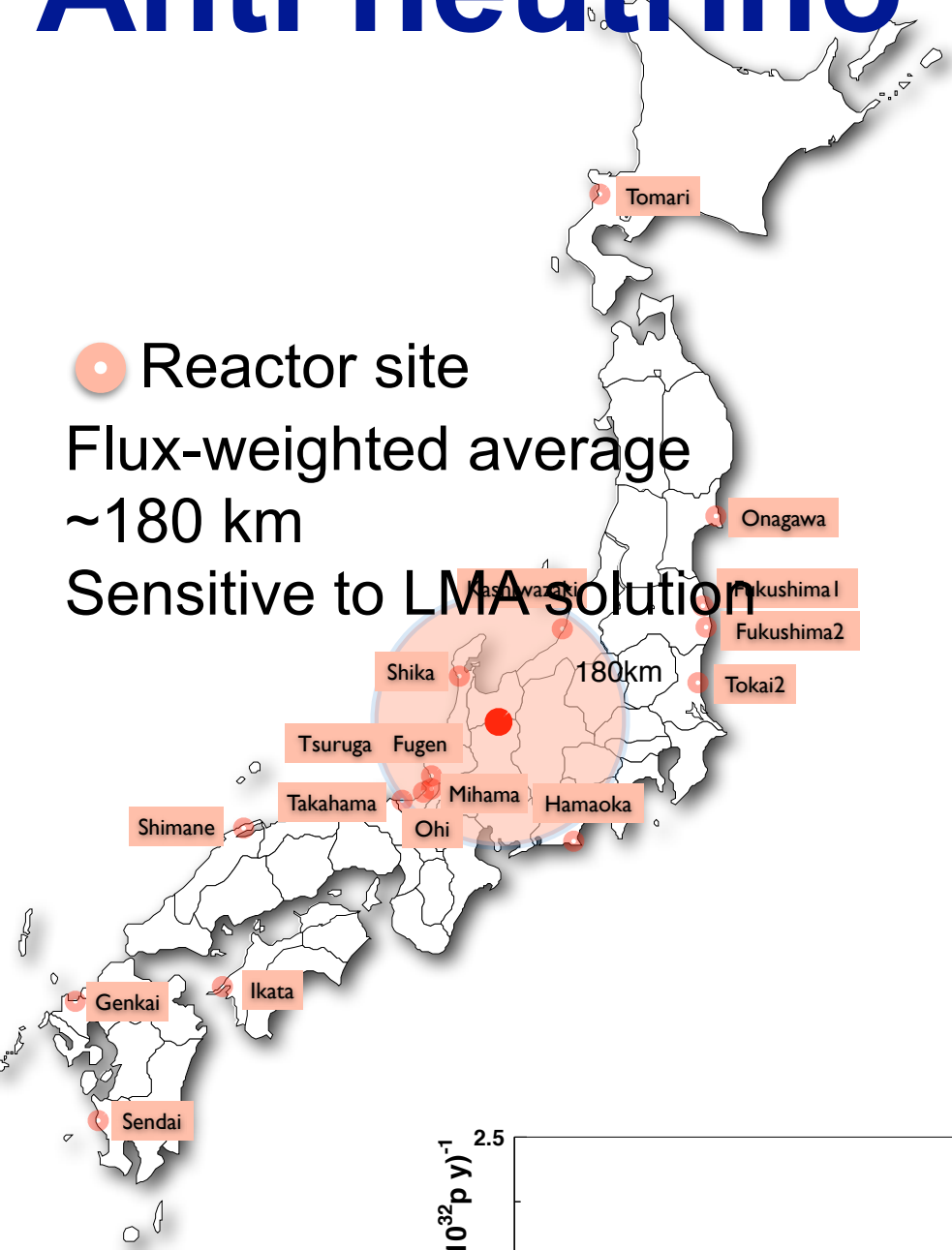
Inverse beta decay → Delayed coincidence



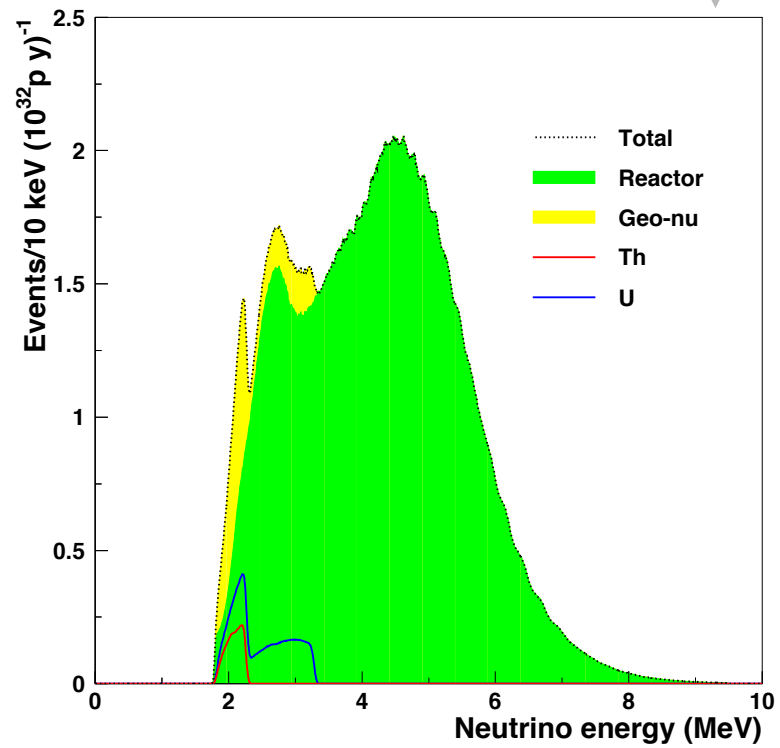
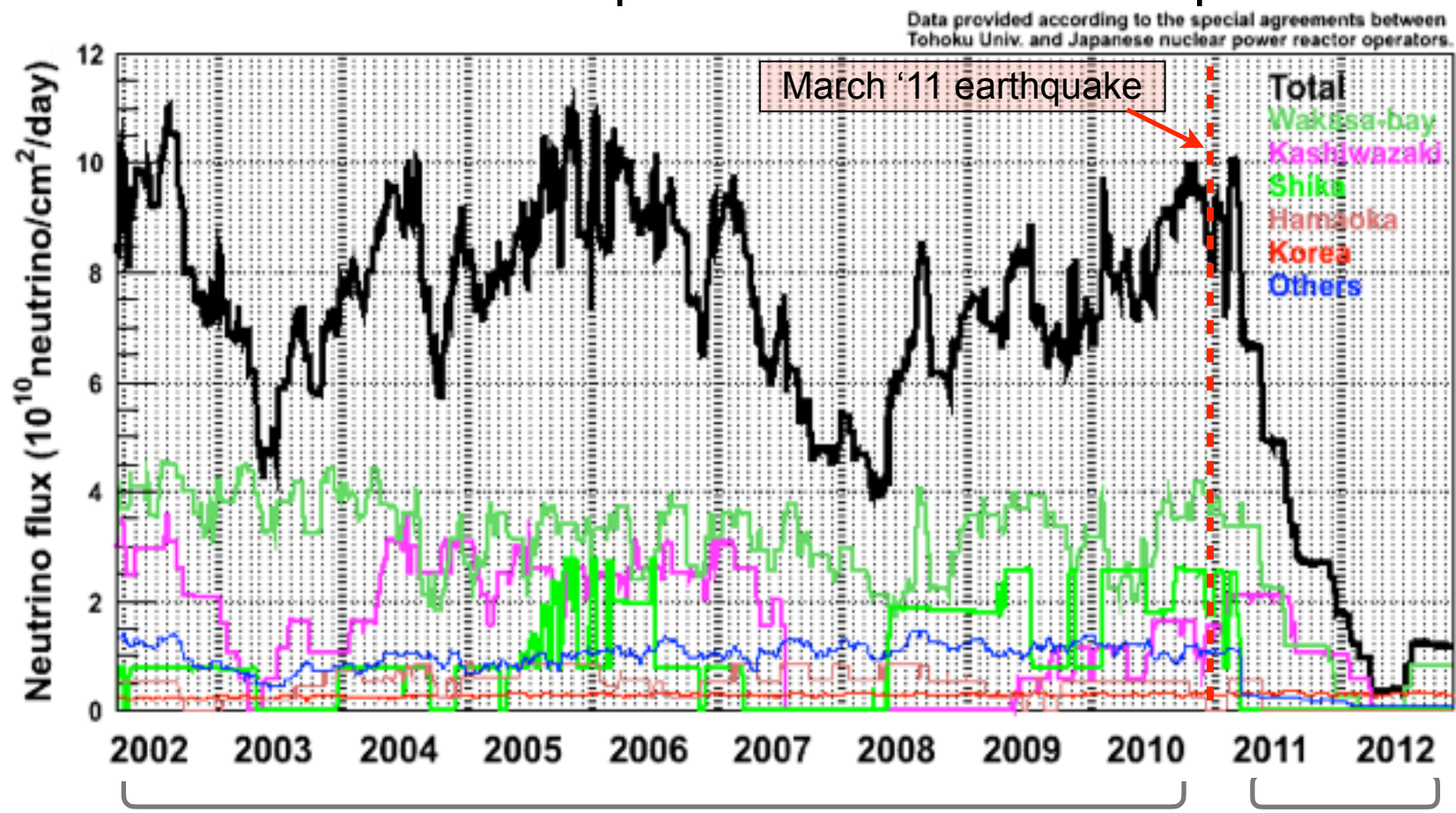
Overview of recent result

Phys. Rev. D **88**, 033001 (2013)

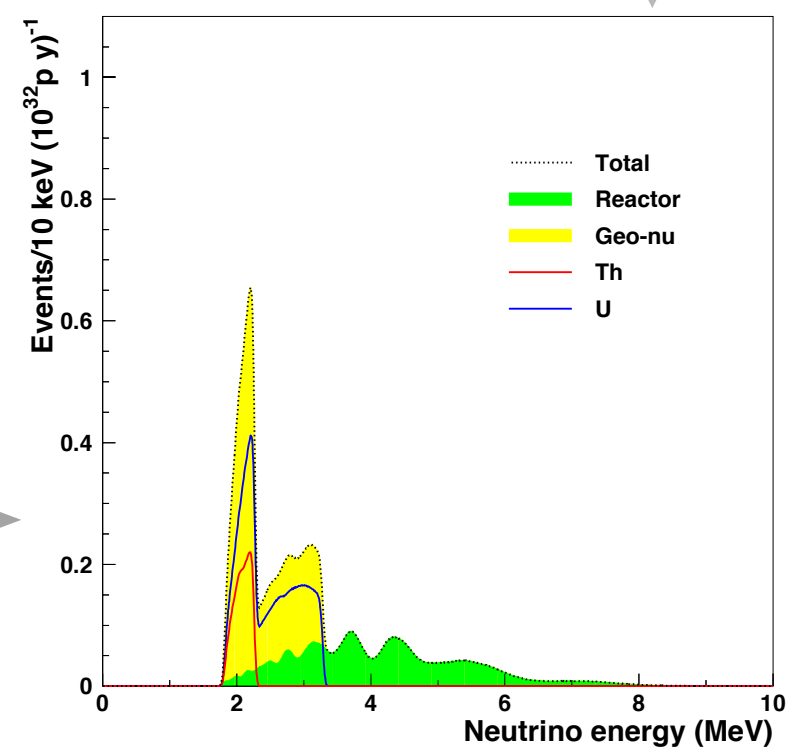
Anti neutrino flux in Kamioka



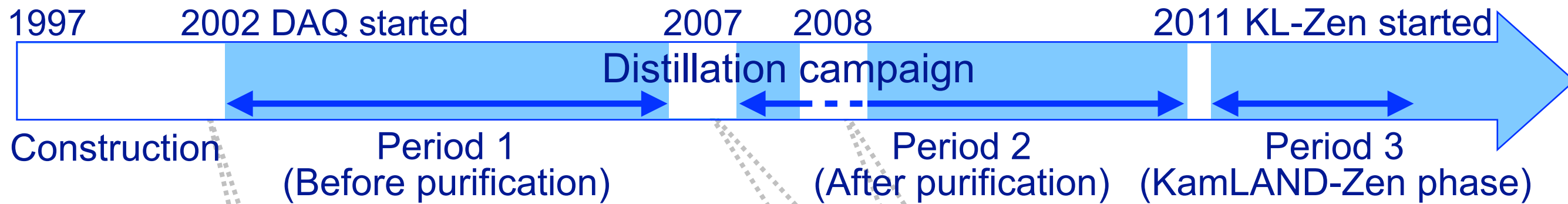
Precise reactor operation data from companies



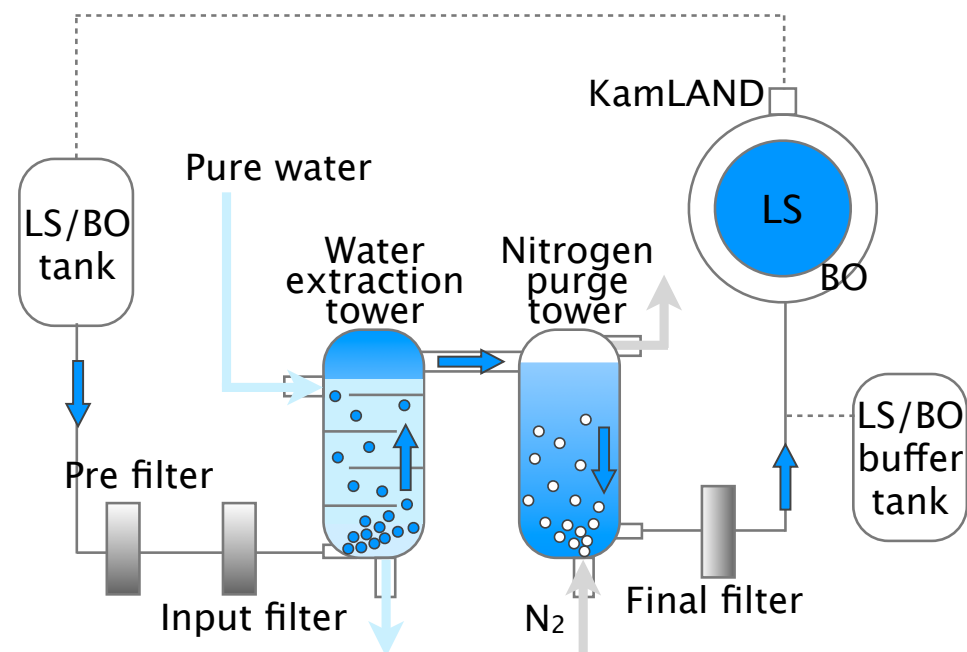
Significant reduction
of anti neutrino flux
after '11 earthquake
(Fukushima accident)



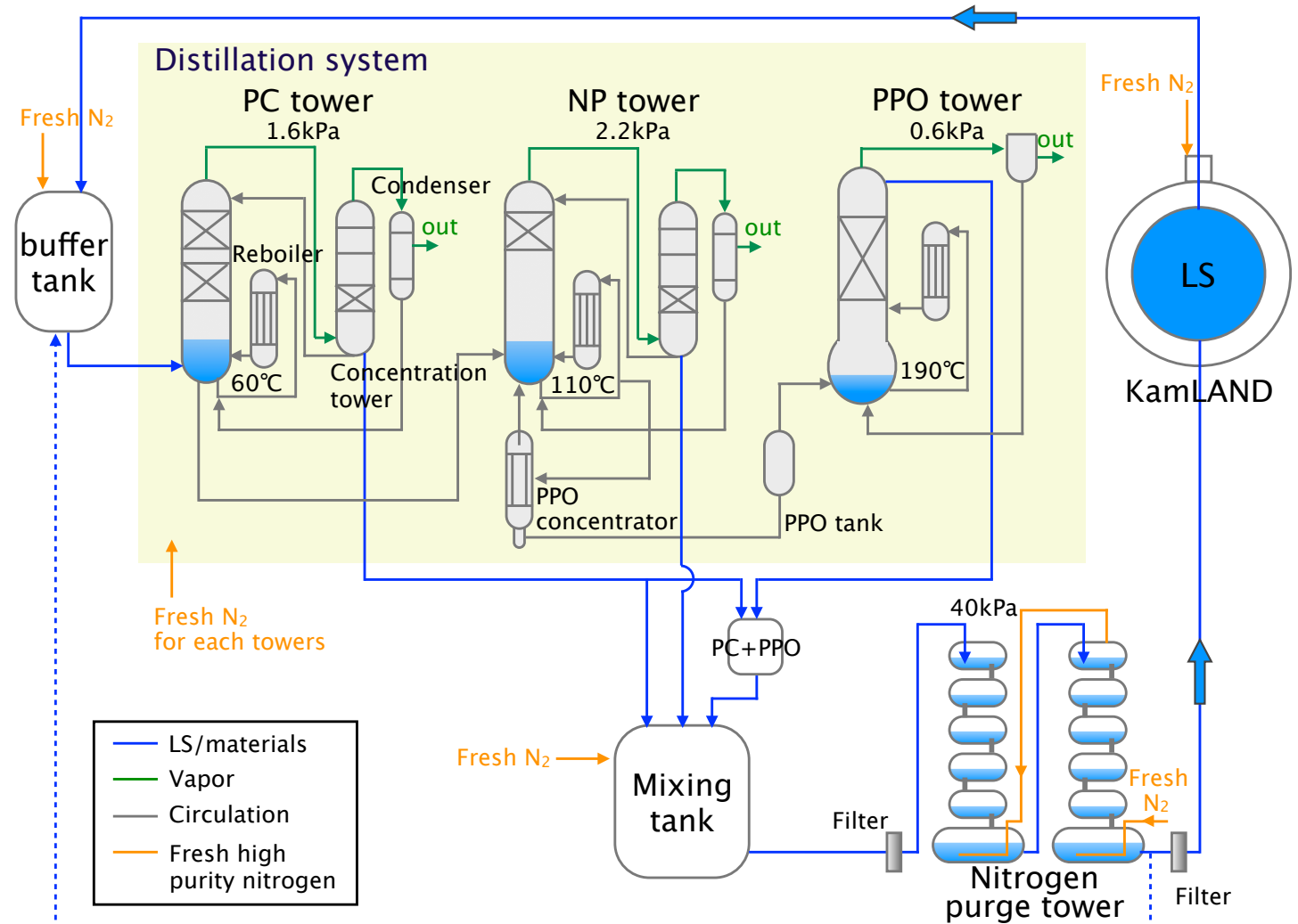
KamLAND operation status



Water extraction



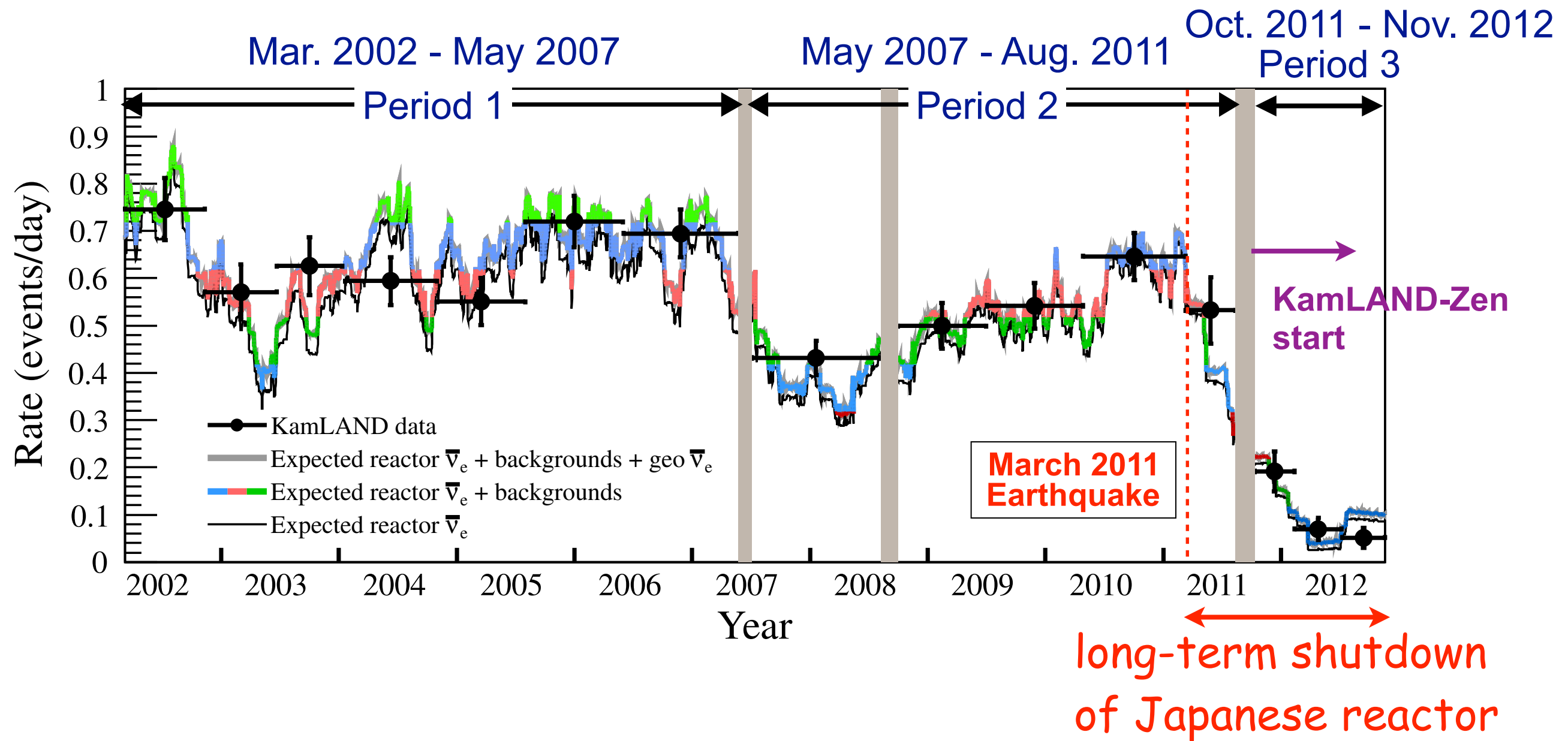
Distillation



Time variation of event rate

$2.6 < E_p < 8.5 \text{ MeV}$

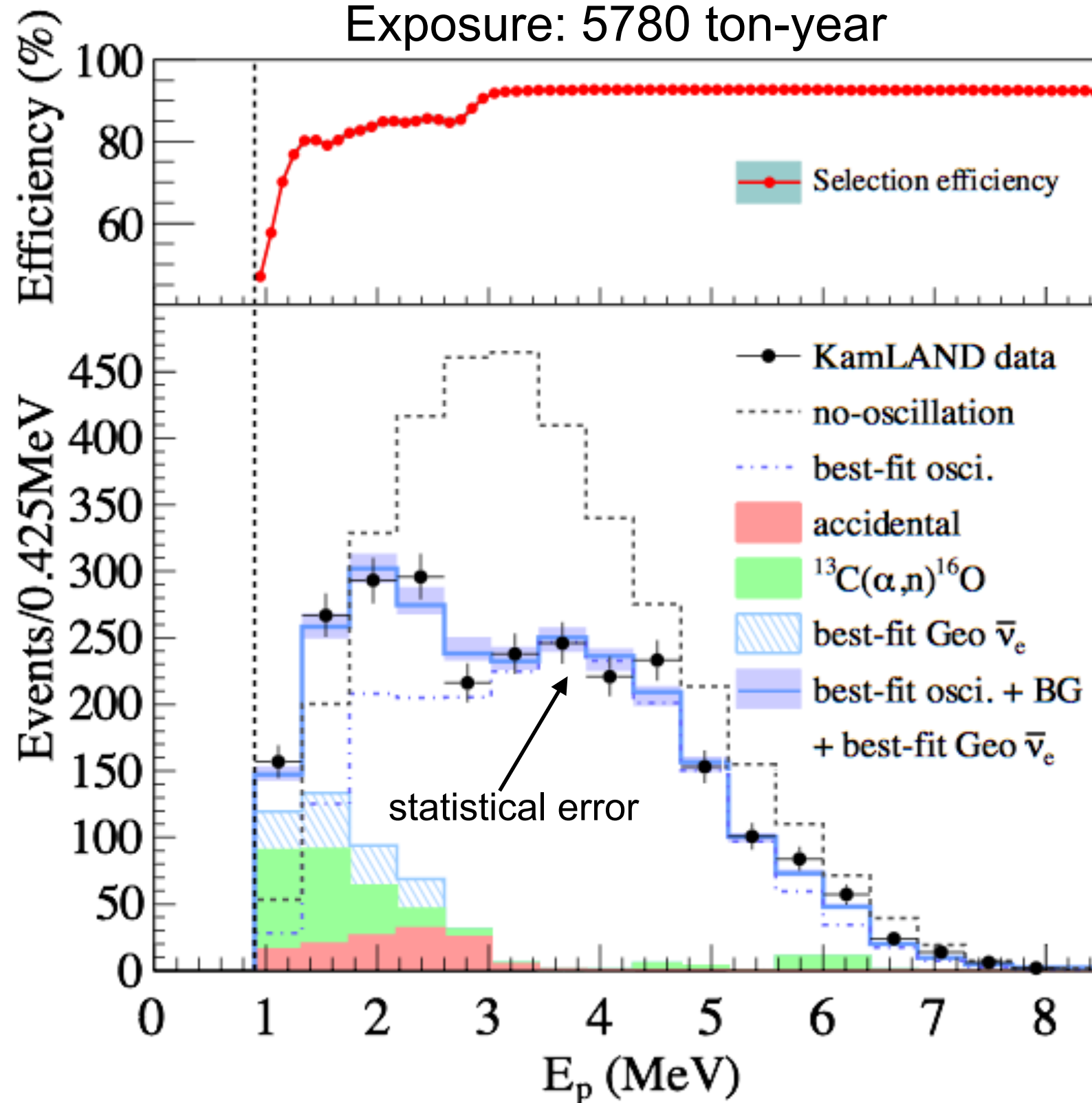
Total livetime
2991 days



Data have good agreement with expected rate

Observed energy spectrum

Exposure: 5780 ton-year



No osci. expected 3564 ± 145

Background
(w/o geo neutrino) 364 ± 31

Observed events **2611**

KamLAND only

$$\Delta m_{21}^2 = 7.54_{-0.18}^{+0.19} \times 10^{-5} \text{eV}^2$$

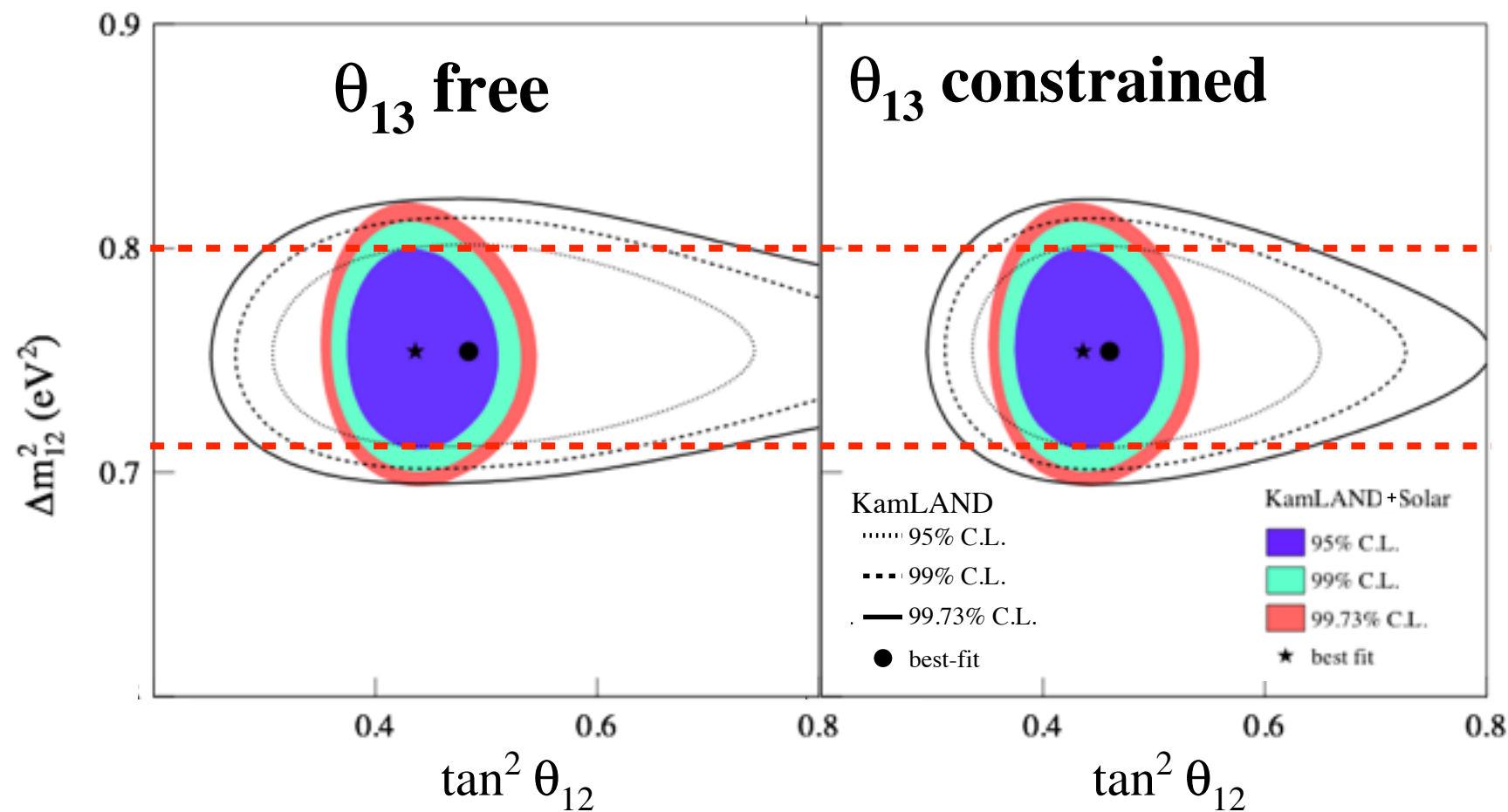
$$\tan^2 \theta_{12} = 0.481_{-0.080}^{+0.092}$$

$$\sin^2 \theta_{13} = 0.010_{-0.034}^{+0.033}$$

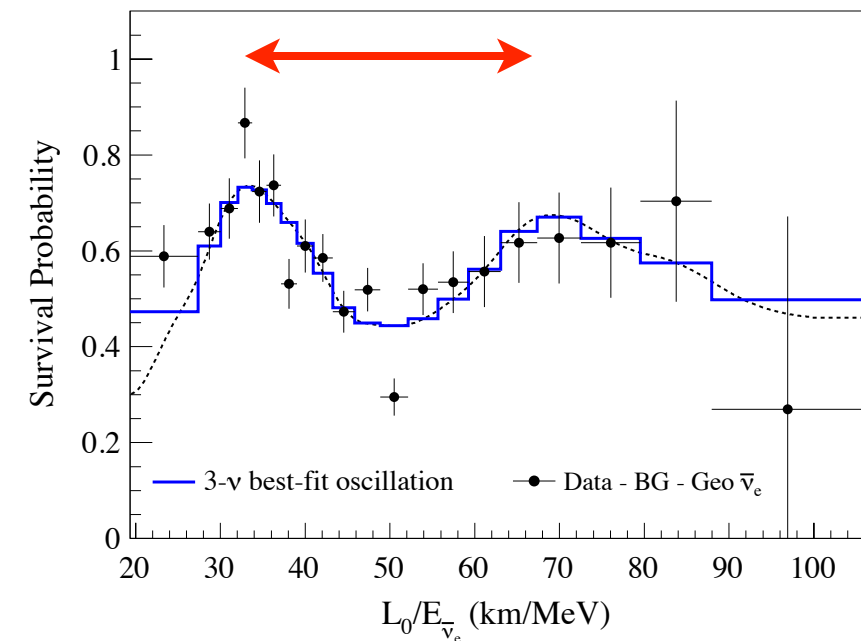
No statistical power to measure 5 MeV bump

Precise Measurement of Δm^2

Δm^2 : systematic uncertainty 1.9%
(dominated by linear energy scale uncertainty)



frequency meas.
by KamLAND



KamLAND+Solar

$$\Delta m^2_{21} = 7.53^{+0.19}_{-0.18} \times 10^{-5} \text{ eV}^2$$

$$\tan^2 \theta_{12} = 0.437^{+0.029}_{-0.026}$$

$$\sin^2 \theta_{13} = 0.023^{+0.015}_{-0.015}$$

KamLAND+Solar+ θ_{13}

$$\Delta m^2_{21} = 7.53^{+0.18}_{-0.18} \times 10^{-5} \text{ eV}^2$$

$$\tan^2 \theta_{12} = 0.436^{+0.029}_{-0.025}$$

$$\sin^2 \theta_{13} = 0.023^{+0.002}_{-0.002}$$

θ_{13} constraint

← insensitive

← no strong impact

Δm^2 is measured at 2.3% precision

Results with Daya-Bay spectrum (w/ 5 MeV bump) is consistent within error

Calibration and energy scale

Analysis plots from dissertation of Hiroko Watanabe (2012) & Koichi Ichimura (2007)

Data sets are different from recent result

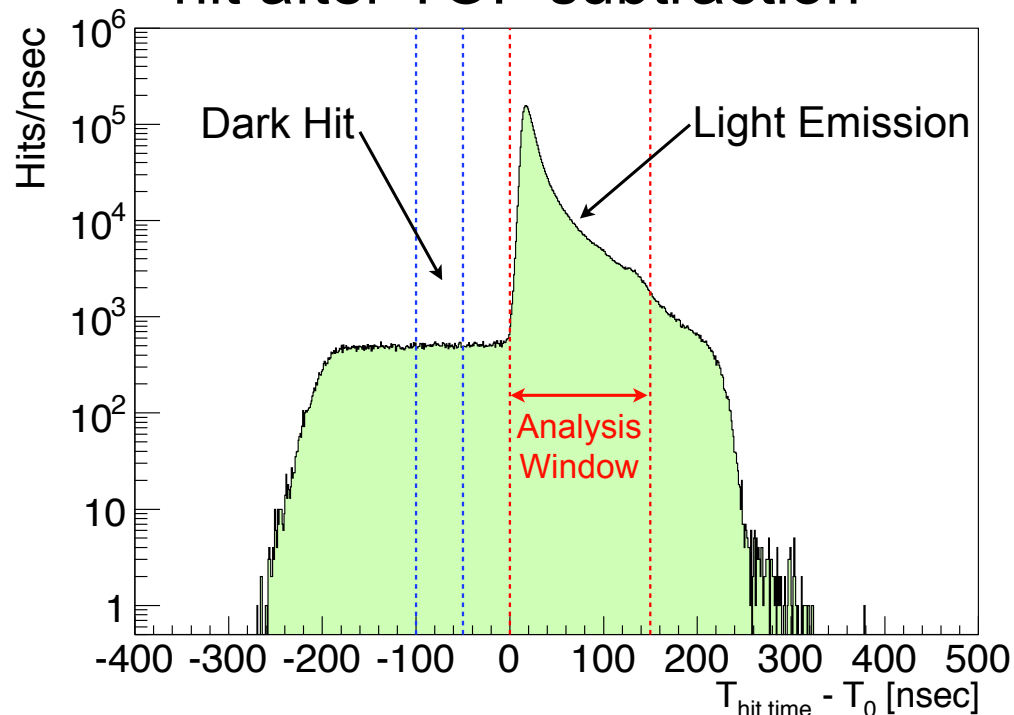
Energy reconstruction

Hit, timing & charge distribution of scintillation photons → “visible energy”

Charge correction

- Gain correction
- Bad channel masking
- Software discriminator threshold 0.3 p.e.
- Dark hit subtraction

Timing distribution of PMTs
hit after TOF subtraction



Energy estimation

→ Maximum likelihood method

Likelihood function

$$L = \prod_i^{\text{no-hit}} P(\text{no-hit}|\mu_i) \prod_i^{\text{hit}} P(\text{hit}|\mu_i) P(q_i|\mu_i) \eta_i(t_i|\mu_i)$$

$$= \prod_i^{\text{no-hit}} \kappa_{i,0}(\vec{R}_{\text{PMT}_i}, \vec{R}_{\text{source}}, E_{\text{vis}}) \prod_i^{\text{hit}} \left[\sum_{j=1}^{\infty} \kappa_{i,j}(\vec{R}_{\text{PMT}_i}, \vec{R}_{\text{source}}, E_{\text{vis}}) f_{i,j}(q_i) \right] \times \eta_i(t_i|\mu_i), \quad (3.24)$$

where

$$\kappa_{i,j} = \begin{cases} \nu_i e^{-\mu_i} = [1 + (1 - \varepsilon)\mu_i] e^{-\mu_i} & (j = 0, \text{no-hit}) \\ \frac{\mu_i^j}{j!} e^{-\mu_i} & (j > 0, \text{hit}) \end{cases} \quad (3.25)$$

$$\mu_i = cE_{\text{vis}} \Omega_{\text{eff}_i}(\vec{R}_{\text{PMT}_i}, \vec{R}_{\text{source}}) + d_i$$

$$\equiv b_i(\vec{R}_{\text{PMT}_i}, \vec{R}_{\text{source}}) E_{\text{vis}} + d_i. \quad (3.26)$$

i : the index for each PMT,

μ_i : expected number of photons hitting i -th PMT including the corrections related to quantum efficiency of PMTs, shadowing effect caused by balloon and ropes, and light attenuation effect.

q_i : the observed charge in the i -th PMT.

$P(\text{no-hit}|\mu_i)$ and $P(\text{hit}|\mu_i)$: The probability density function of i -th PMT hit information. It is denoted by $\kappa_{i,j}$ provided by the Poisson distribution with μ_i as a parameter (Eq. (3.26)). j means actual number of photons

Energy calibration overview

Source

1. off-axis (4pi) ^{60}Co , ^{68}Ge , ^{203}Hg , $^{241}\text{Am}^9\text{Be}$ ($^{210}\text{Po}^{13}\text{C}$)

B. E. Berger et al., 2009 JINST 4 P04017

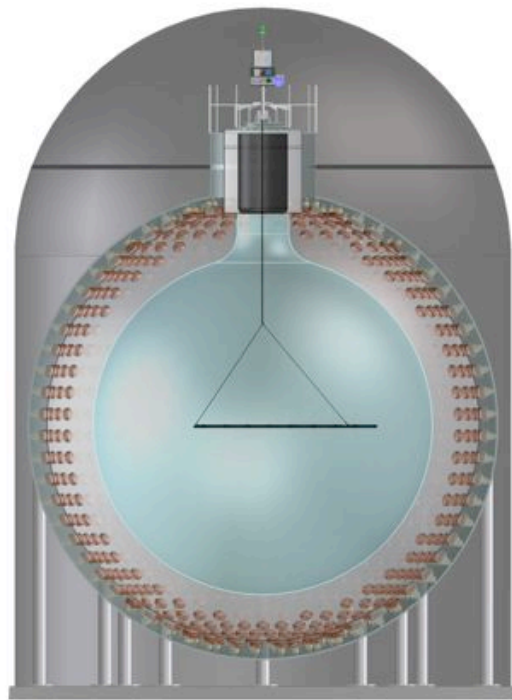


Figure 1. Illustration of the calibration system in the KamLAND detector: A radioactive source was attached to one end of the pole. It was positioned throughout the fiducial volume by adjusting the orientation and length of the pole. Additional ^{60}Co pin sources, used for monitoring the pole position, were located along the pole. Two cables and a spool system manipulated the pole position and provided electrical connections to instrumentation in the pole. Access to the detector and manipulation of the system was through a glovebox on top of the chimney.

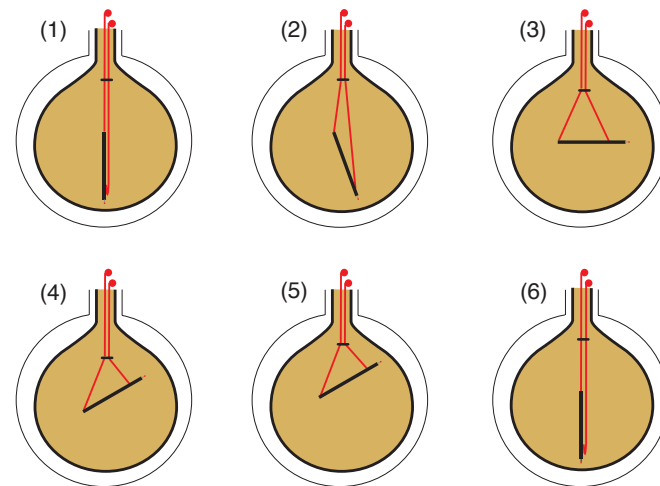


Figure 2. A typical deployment sequence for off-axis calibration: (1) During insertion into the detector, the pole was vertically suspended from the far cable with some slack in the near cable. (2) Once the pole was inside the detector, the near cable was raised, which removed the slack and pulled the pole off axis. (3) The far cable was then lowered and the near cable was raised to move the pole to the horizontal. (4) The near cable was shortened to bring the pole above the horizontal. (5) The far and near cables were raised simultaneously to bring the source closer to the balloon. (6) To prepare the pole for retraction, the near cable was lowered to return the pole to vertical.

2. z-axis ^{60}Co , ^{68}Ge , ^{203}Hg , $^{241}\text{Am}^9\text{Be}$, ^{137}Cs

T.I. Banks et al. NIM A 769 (2015) 88–96

Others

Spallation neutron capture event
(2.225 MeV gamma)

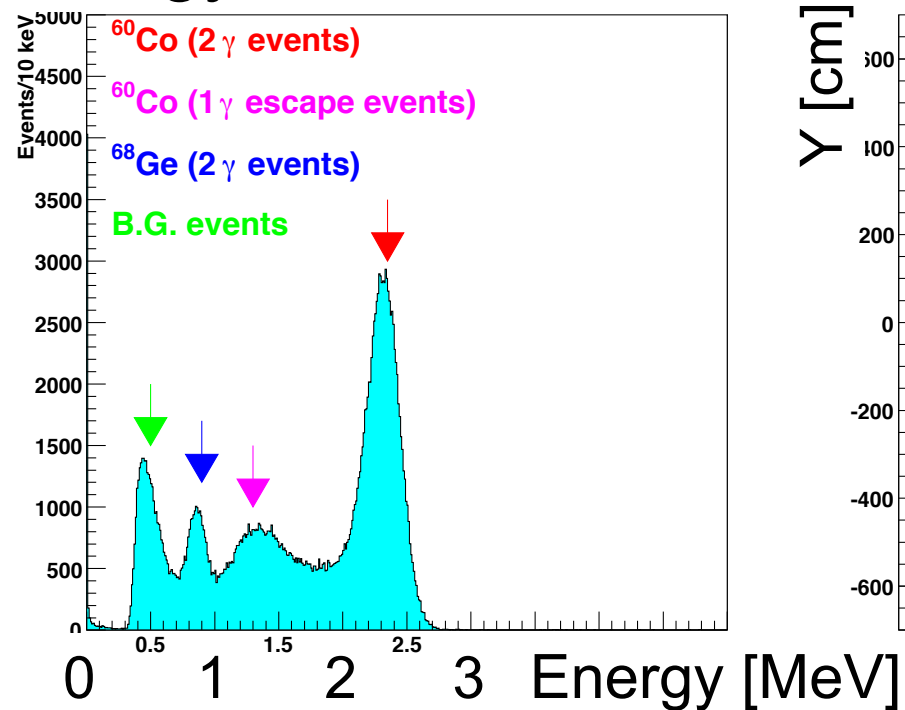
What we check:

- Position dependence
- Time variation
- Energy non-linearity

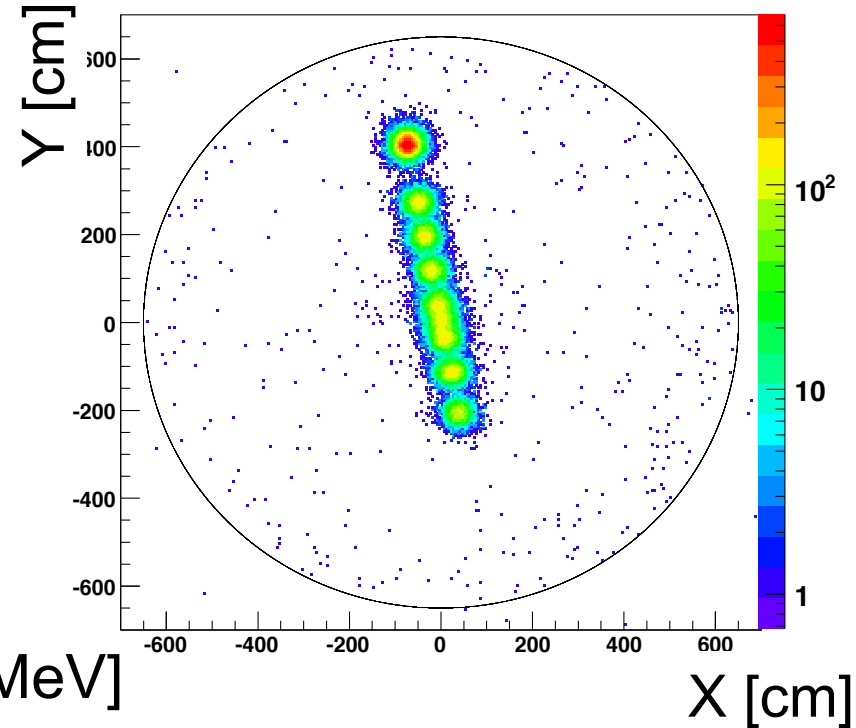
4pi calibration | example

-Checked θ , φ , R and energy deviation

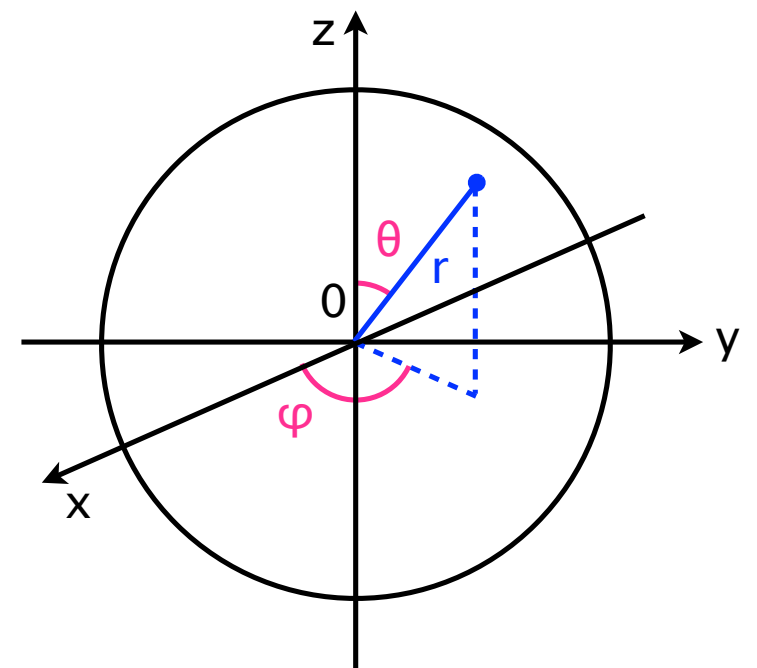
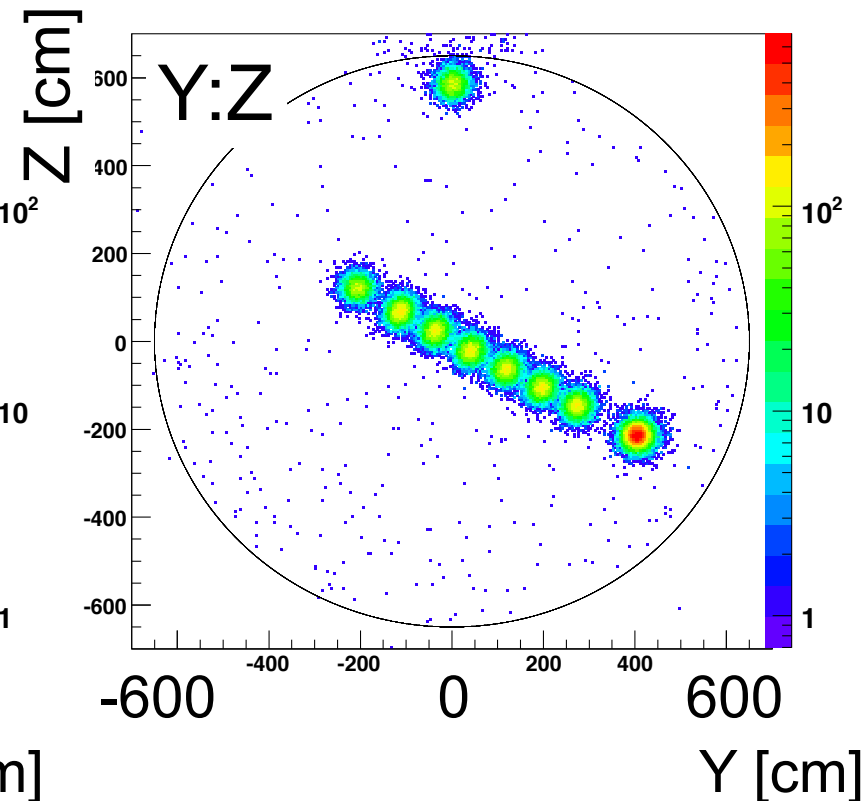
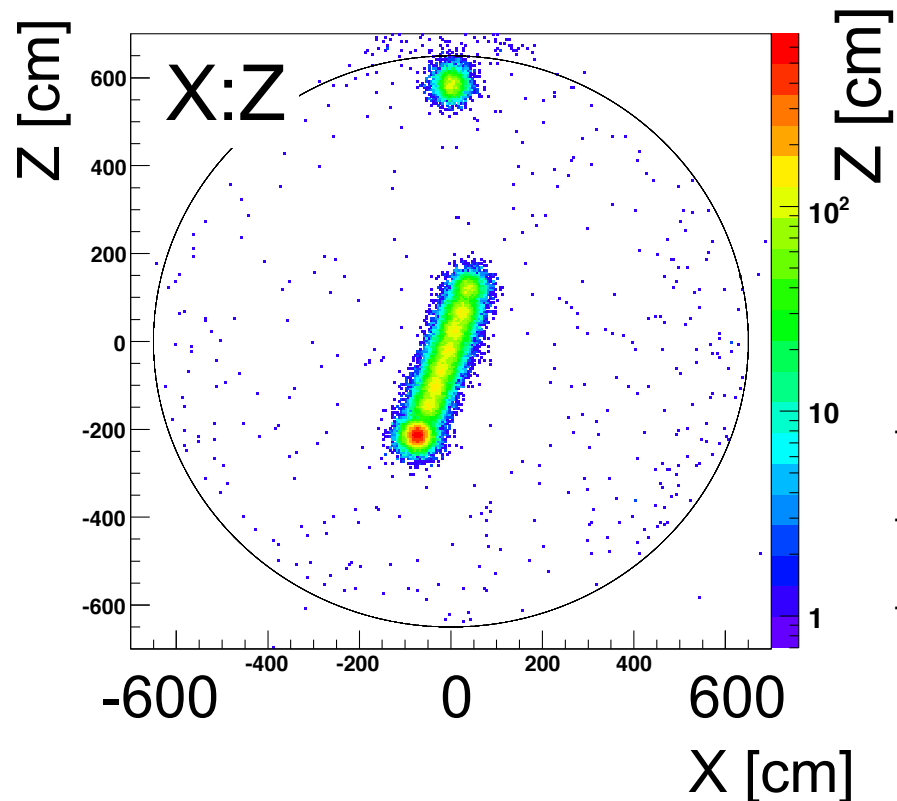
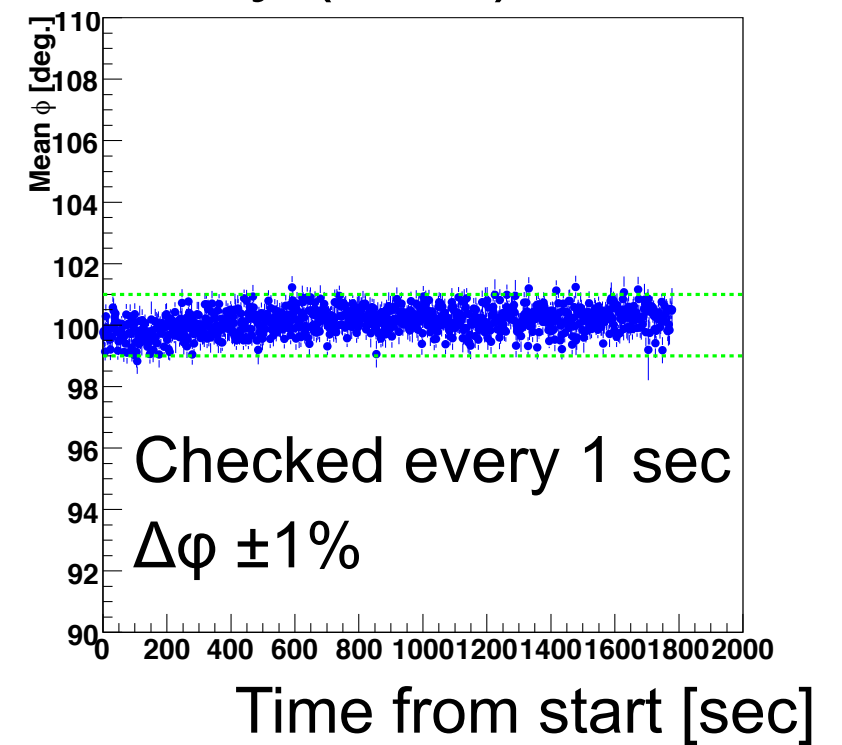
Energy



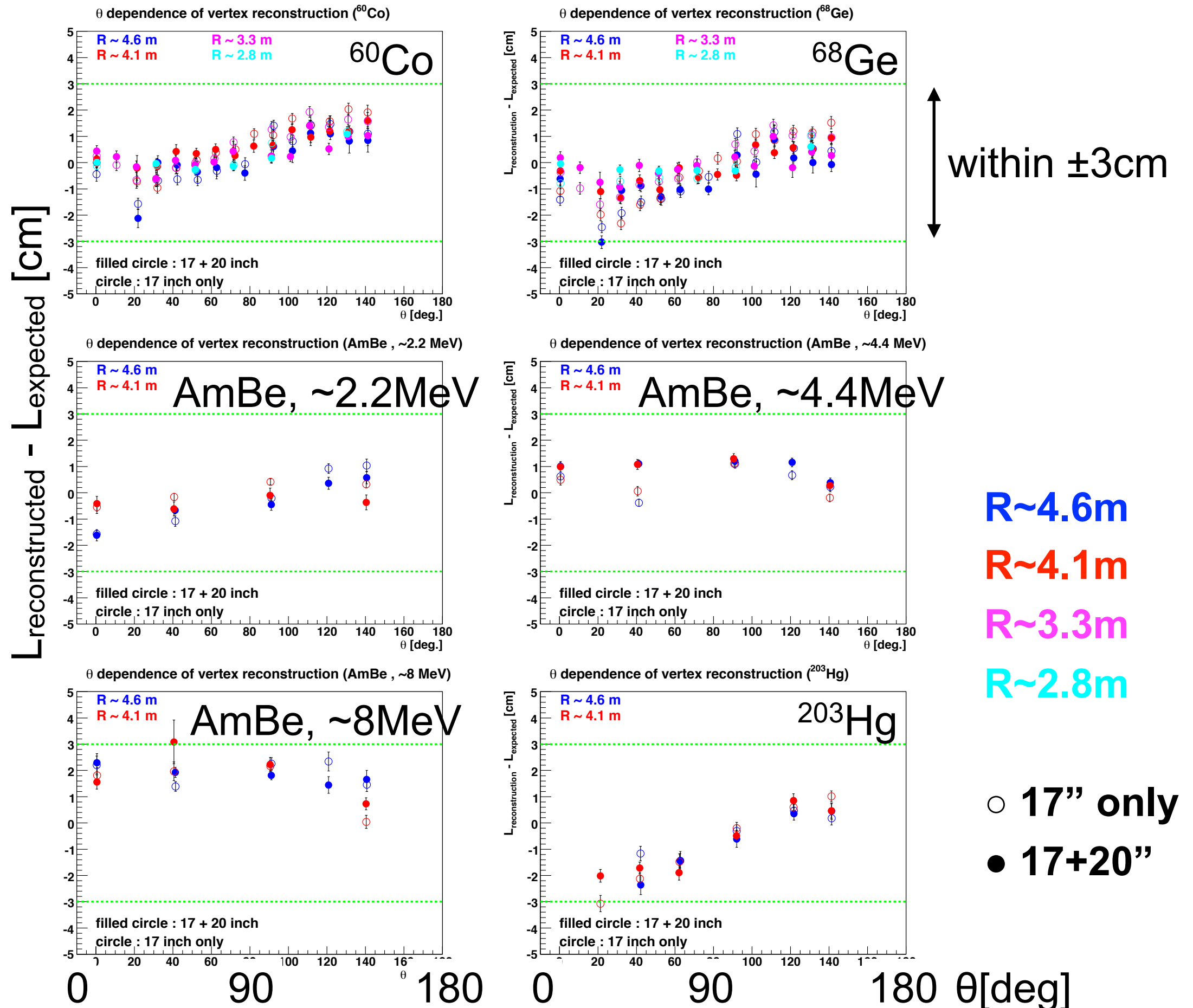
X:Y



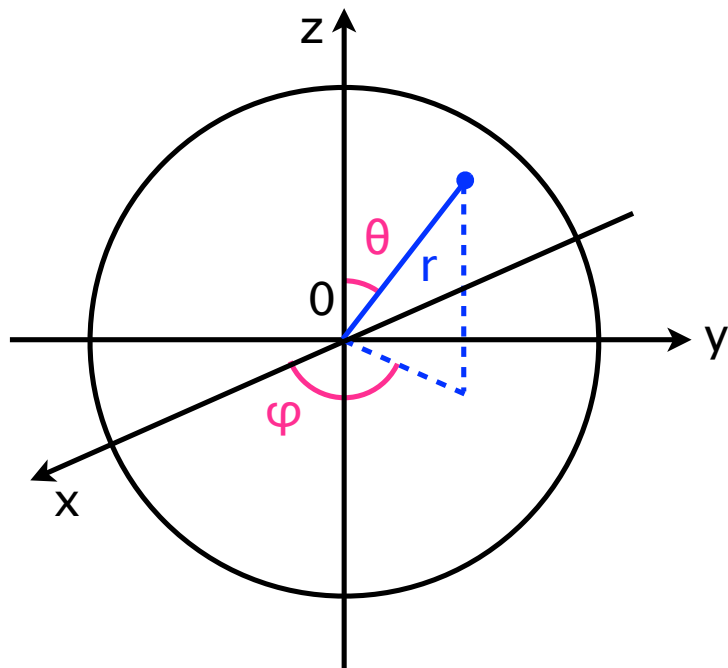
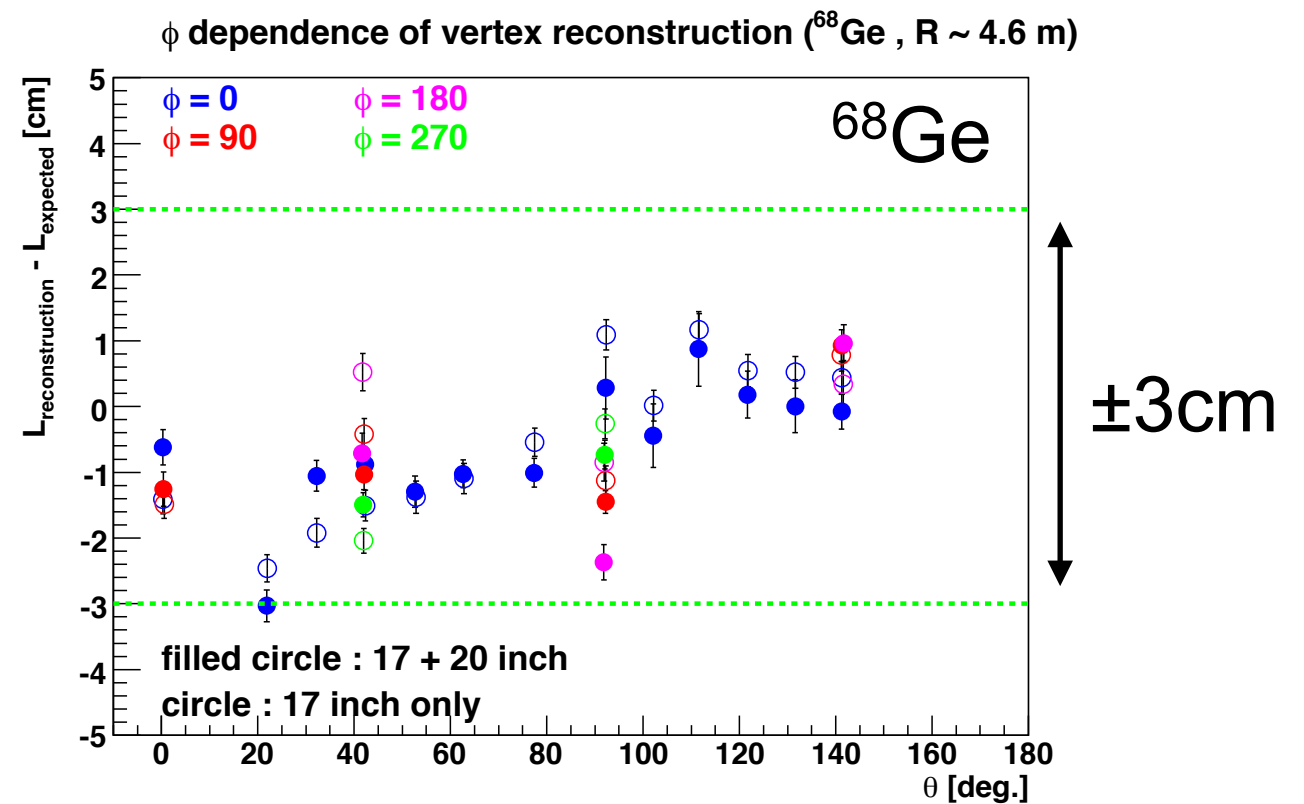
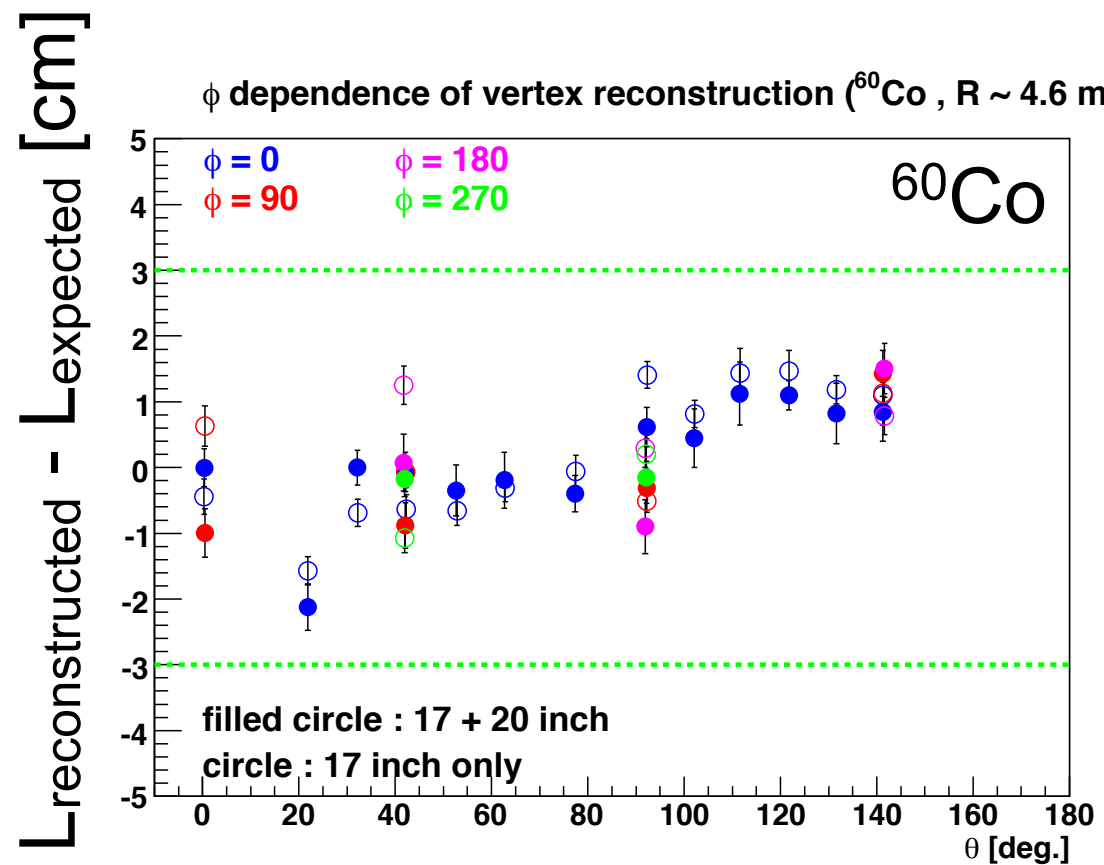
Stability (^{60}Co)



Vertex calibration | 4pi | theta



Vertex calibration | 4pi | phi



$\phi=0$

$\phi=90$

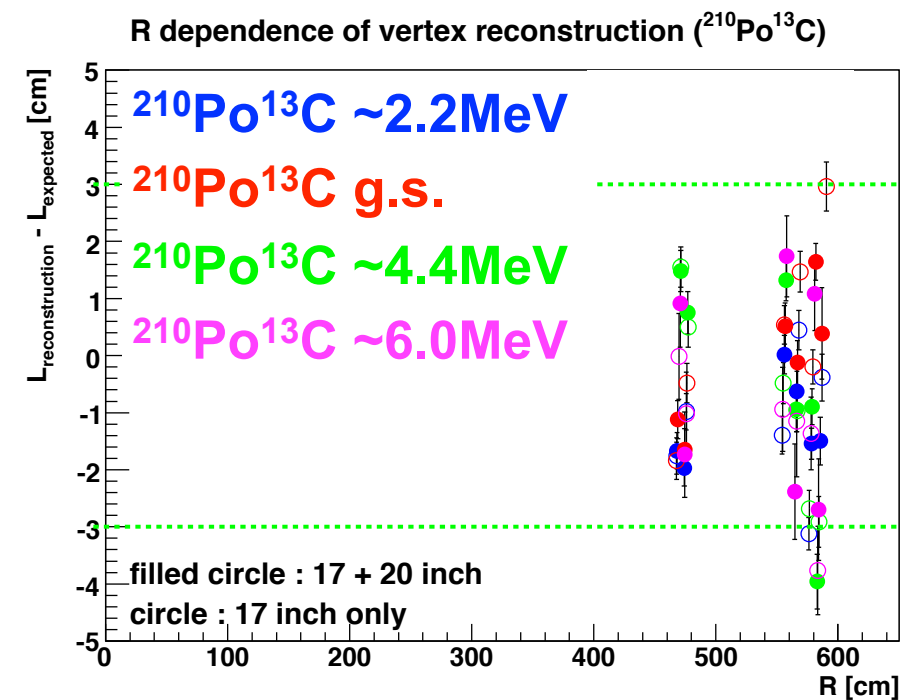
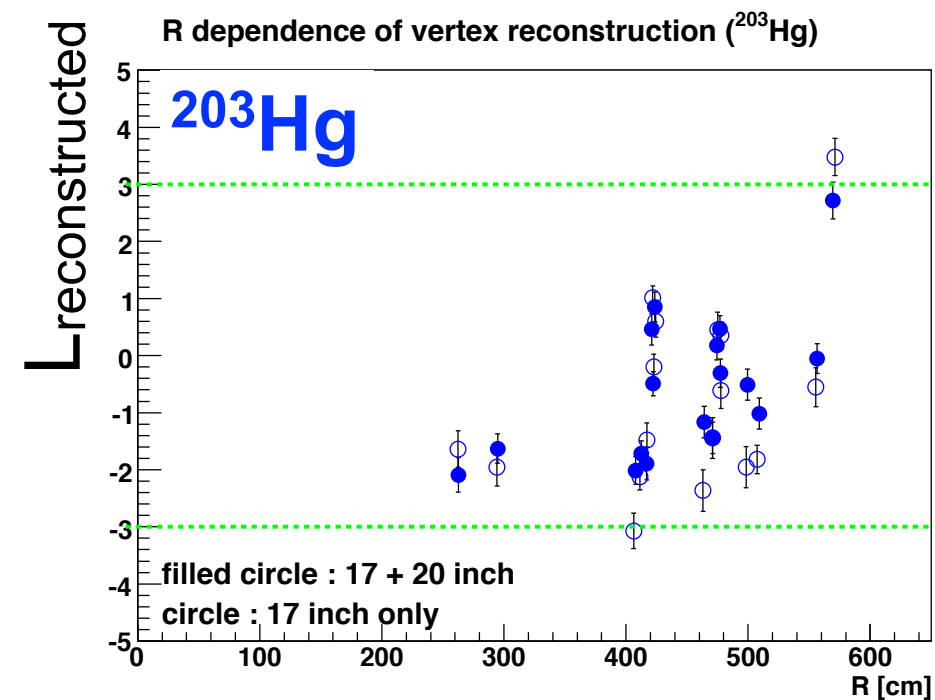
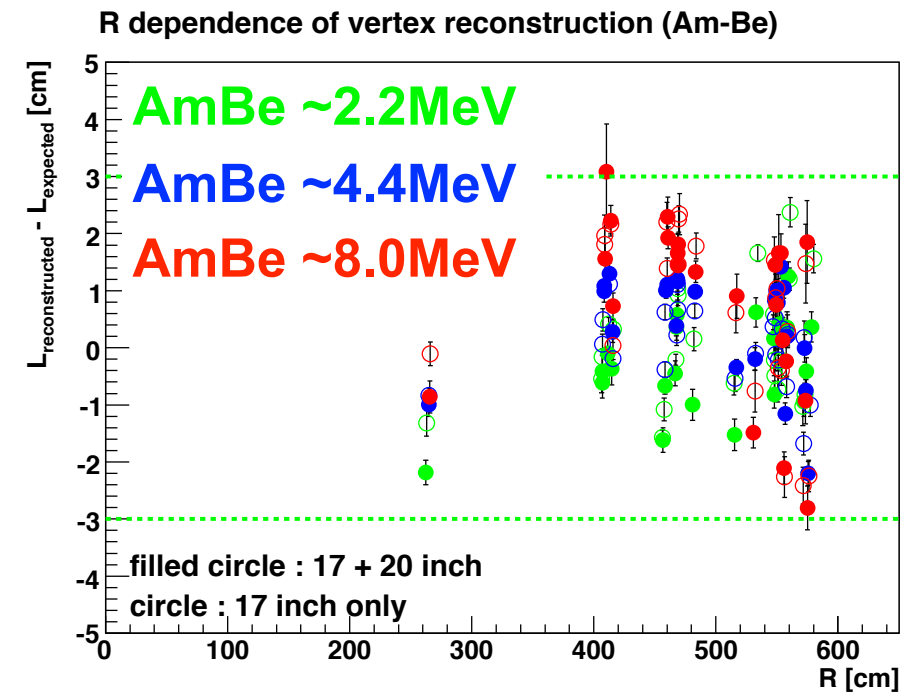
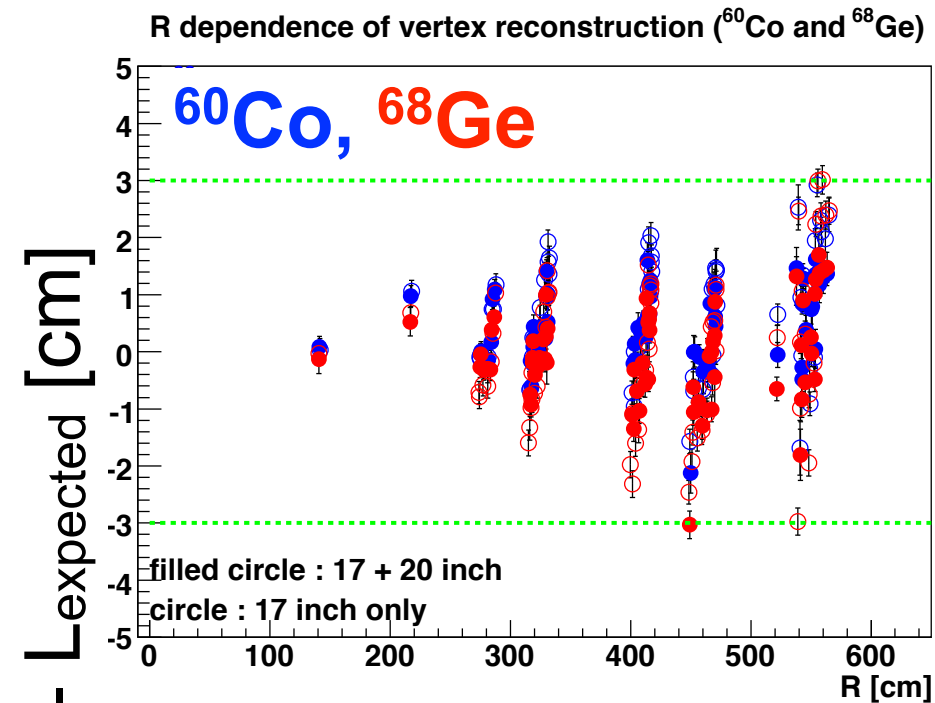
$\phi=180$

$\phi=270$

○ 17" only

● 17+20"

Vertex calibration | 4pi | R



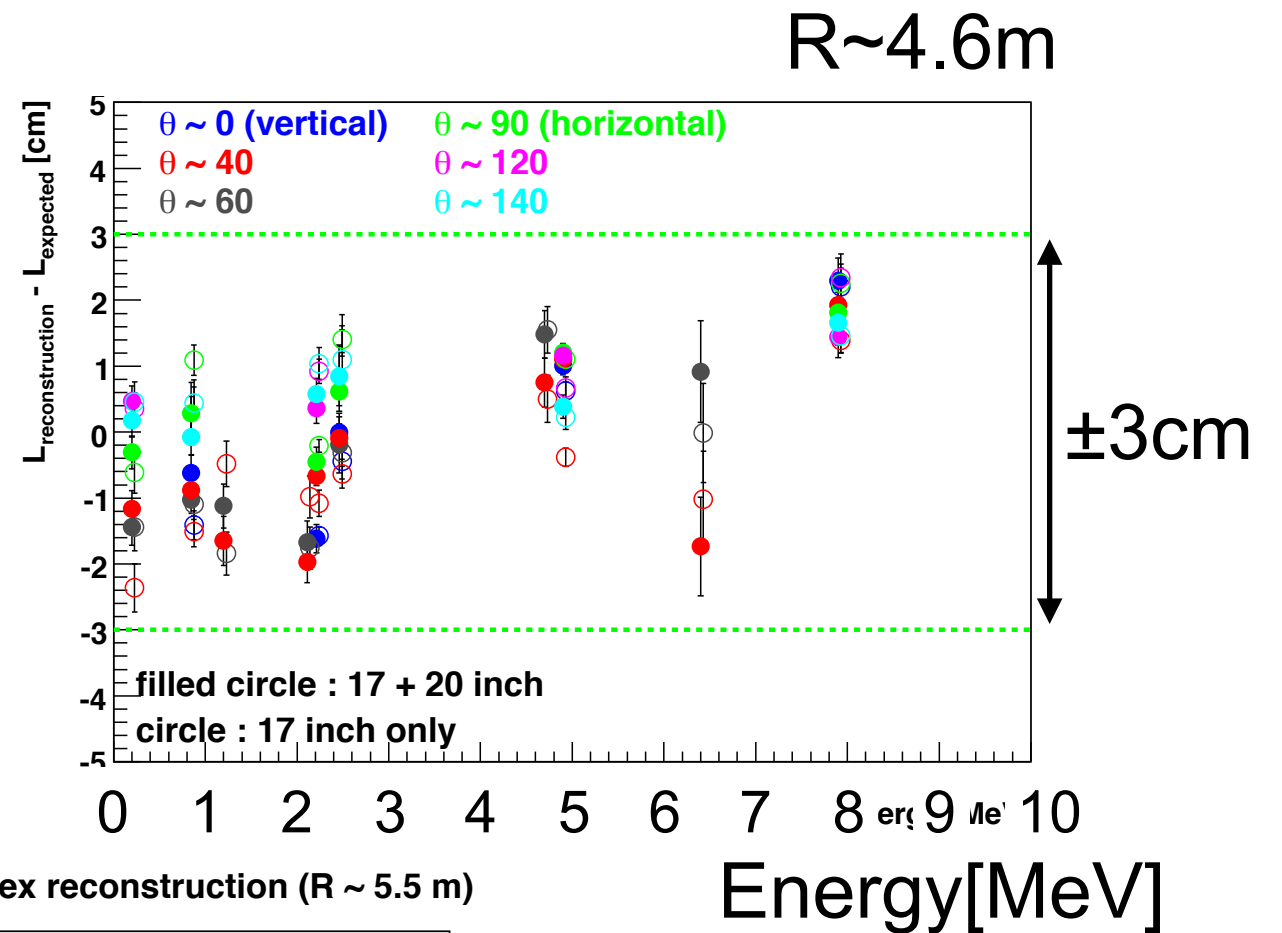
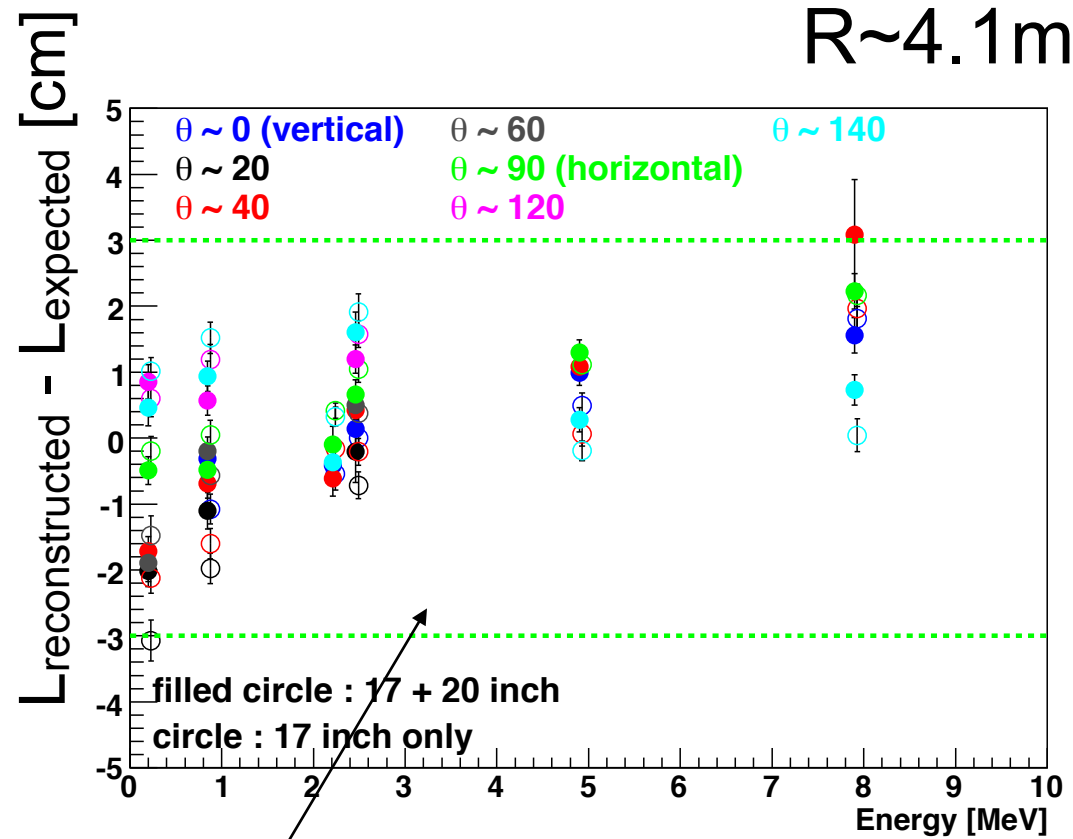
○ 17" only

● 17+20"

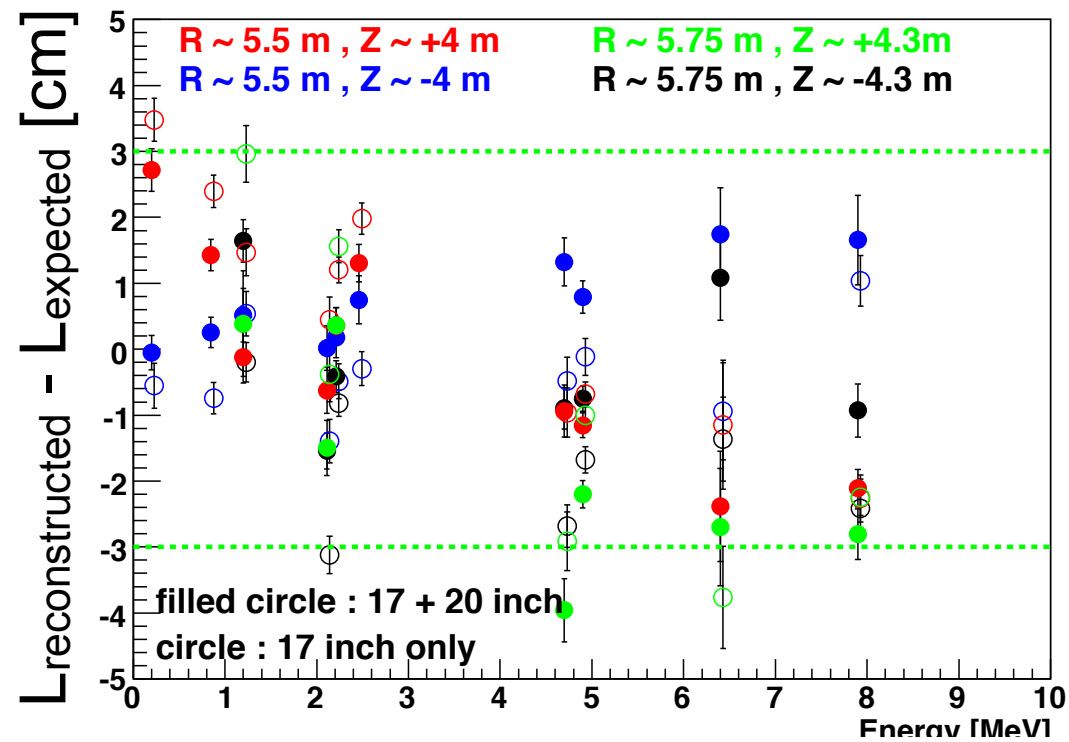
$\pm 3\text{cm}$

The bias $(R, \theta, \varphi) < 3\text{cm} \rightarrow$ Vertex uncertainty for FV $\sim 1.6\%$

Vertex calibration | 4pi | energy



Energy dependence of vertex reconstruction (R ~ 5.5 m)



R~5.5, 5.75m

R~5.5m, Z~+4m

R~5.5m, Z~-4m

R~5.75m, Z~+4.3m

R~5.75m, Z~-4.3m

$\theta \sim 0$ (vertical)

$\theta \sim 20$

$\theta \sim 40$

$\theta \sim 60$

$\theta \sim 90$ (horizontal)

$\theta \sim 120$

$\theta \sim 140$

Energy [MeV]

Energy deviation | 4pi | energy

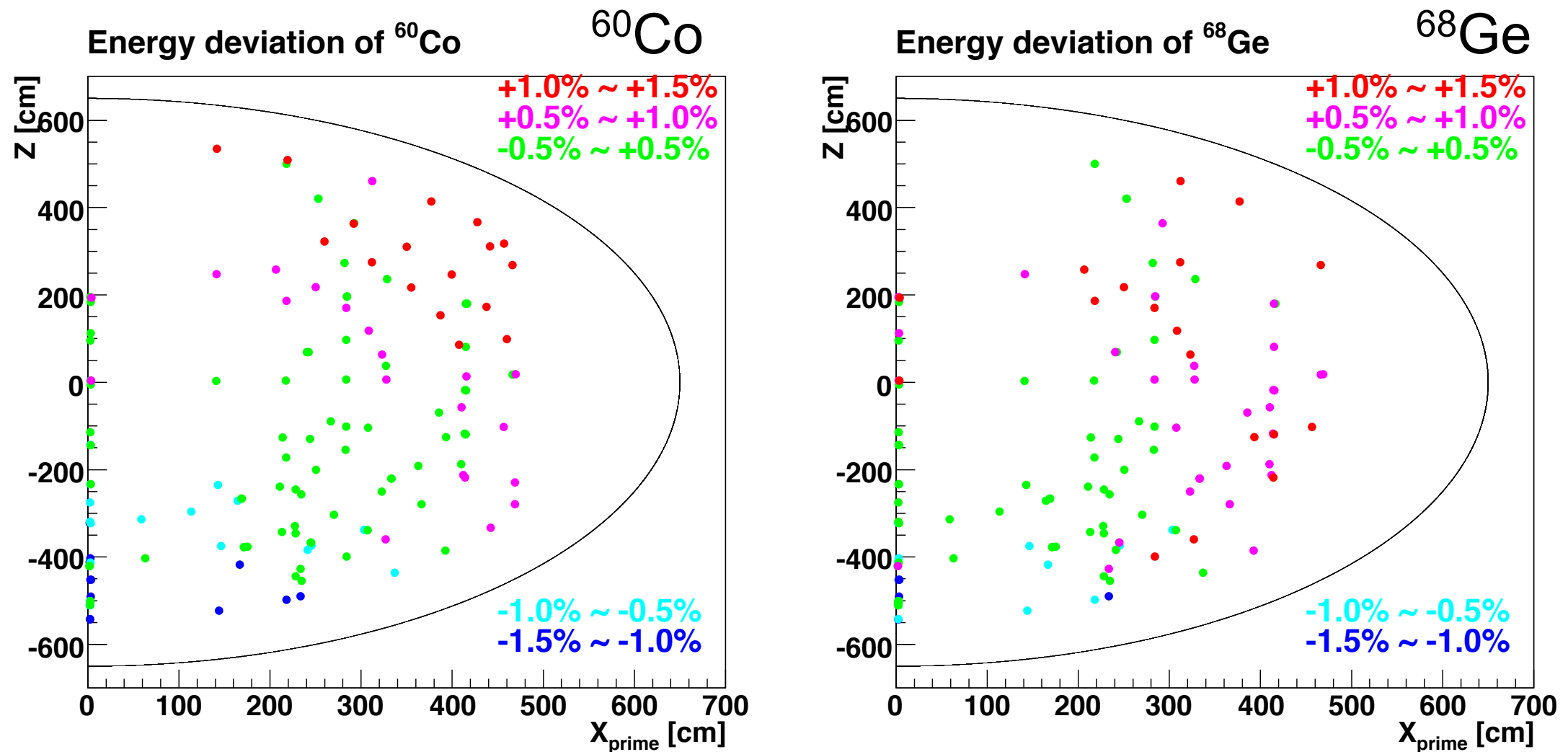


Figure 3.46: Energy deviation of 4π data. Each circle corresponds to the deviation written in the figure. (Left) ^{60}Co energy deviation. (Right) ^{68}Ge energy deviation. Energy deviation is within $\pm 1.5\%$ for ^{60}Co and ^{68}Ge .

Energy calibration | z-axis

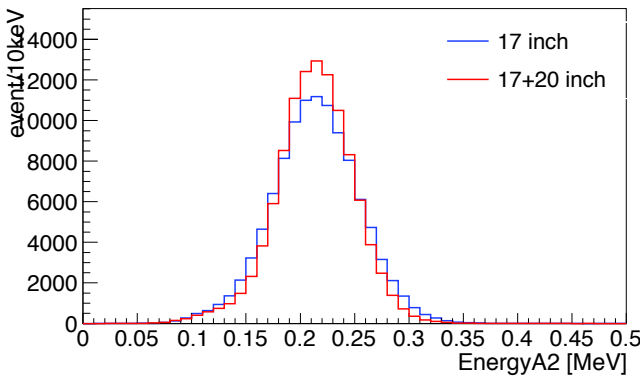
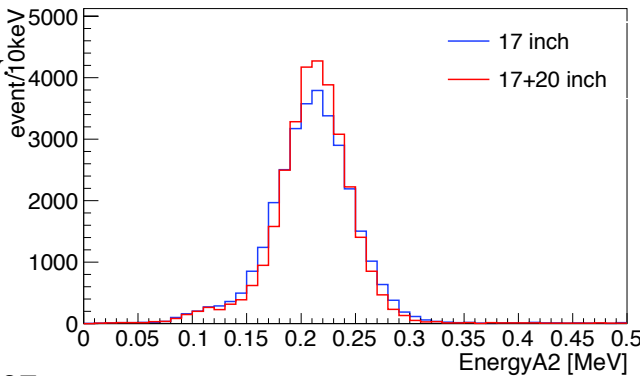
Before Purification

After Purification

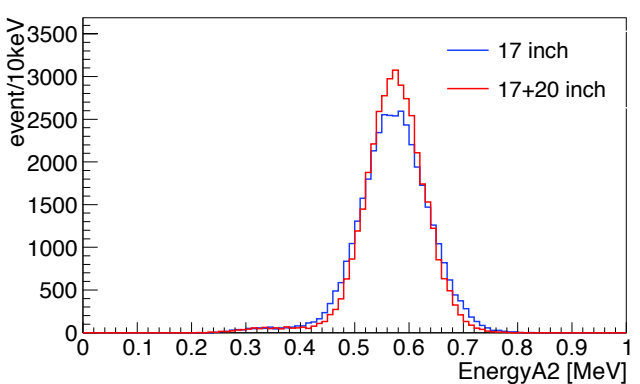
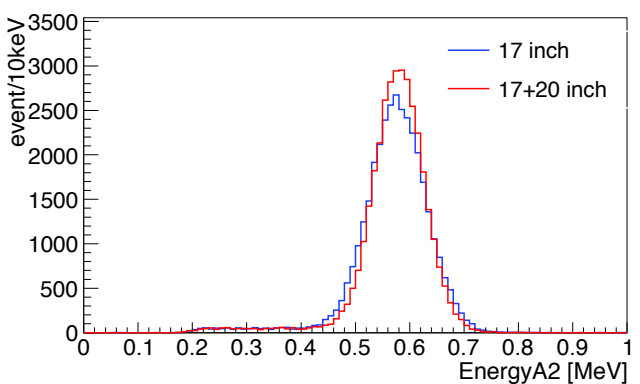
Table 3.2: Checking sources for visible energy reconstruction quality

source	particle type	energy [MeV]
^{203}Hg	γ	0.2792
^{137}Cs	γ	0.6616
^{65}Zn	γ	1.1116
^{68}Ge	γ	0.511×2
^{60}Co	γ	1.1732, 1.3325
$^{241}\text{Am}^9\text{Be}$	γ, n	4.4, $n < 10$
$^{210}\text{Po}^{13}\text{C}$	γ, n	6.13, $n < 7.5$
$np \rightarrow d\gamma$	γ	2.22457

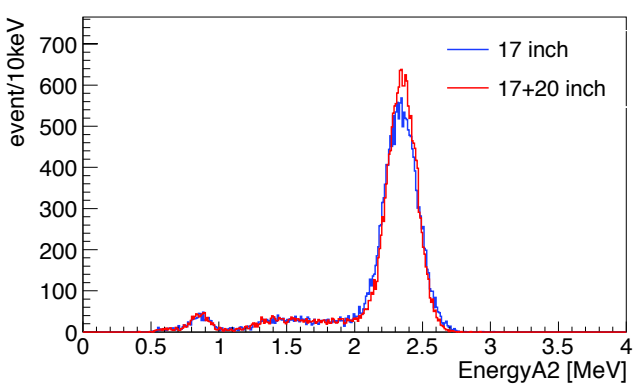
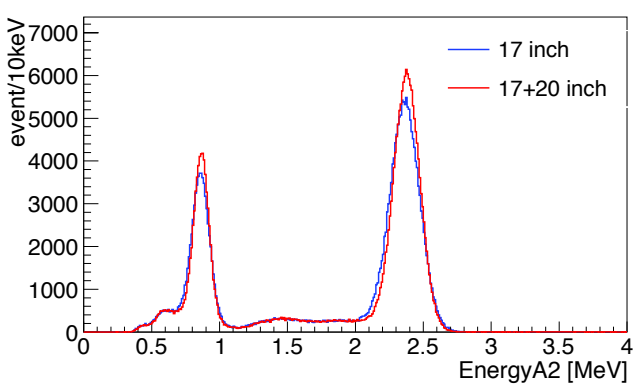
^{203}Hg (1γ , 279 keV)



^{137}Cs (1γ , 661.7 keV)



^{68}Ge (2γ , 511.0 keV $\times 2$), ^{60}Co (2γ , 1173.2 keV + 1332.5 keV)



Am/Be (γ , 4438 keV)

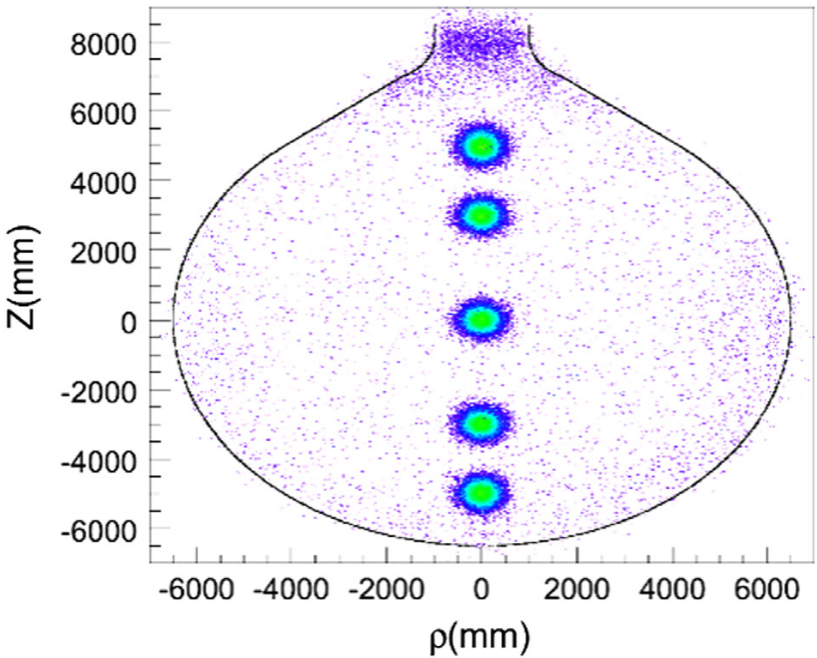
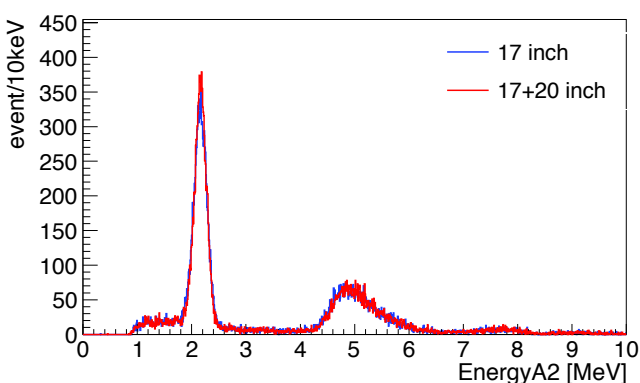
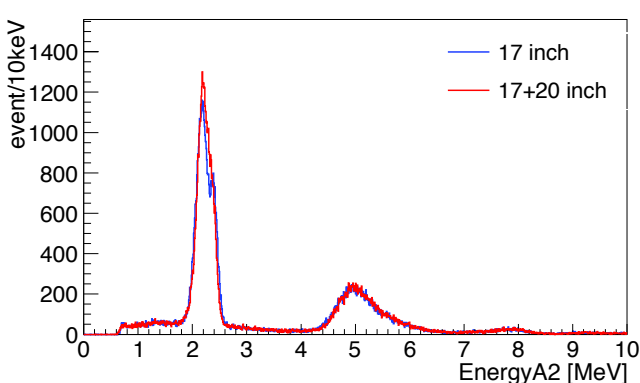
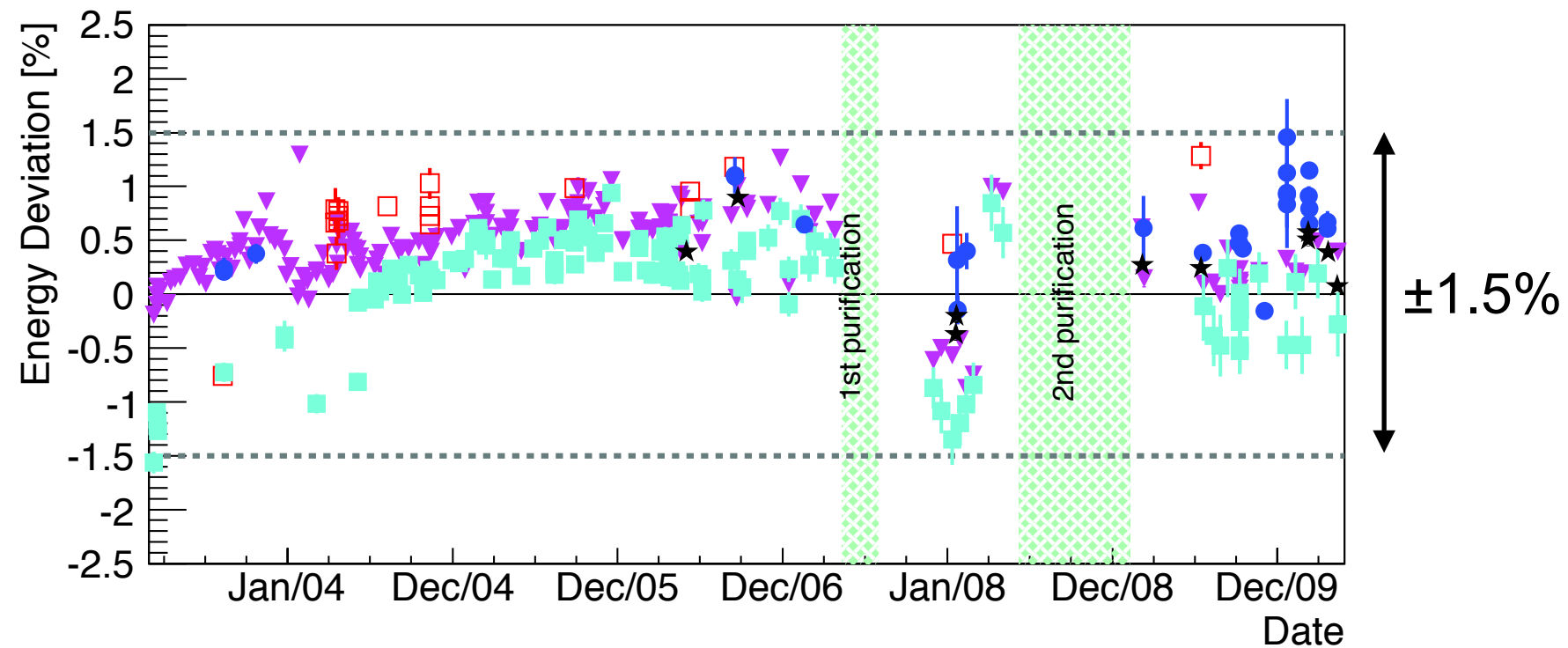


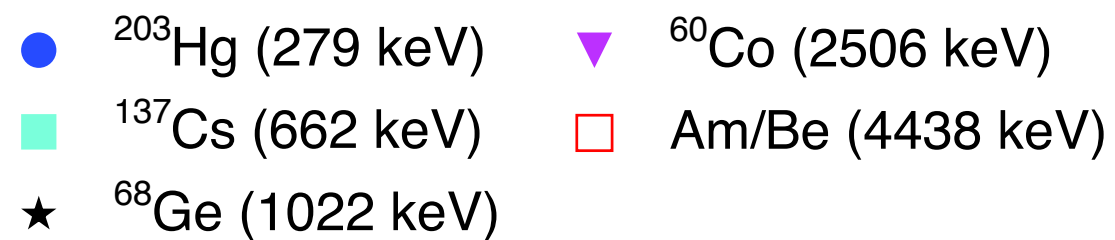
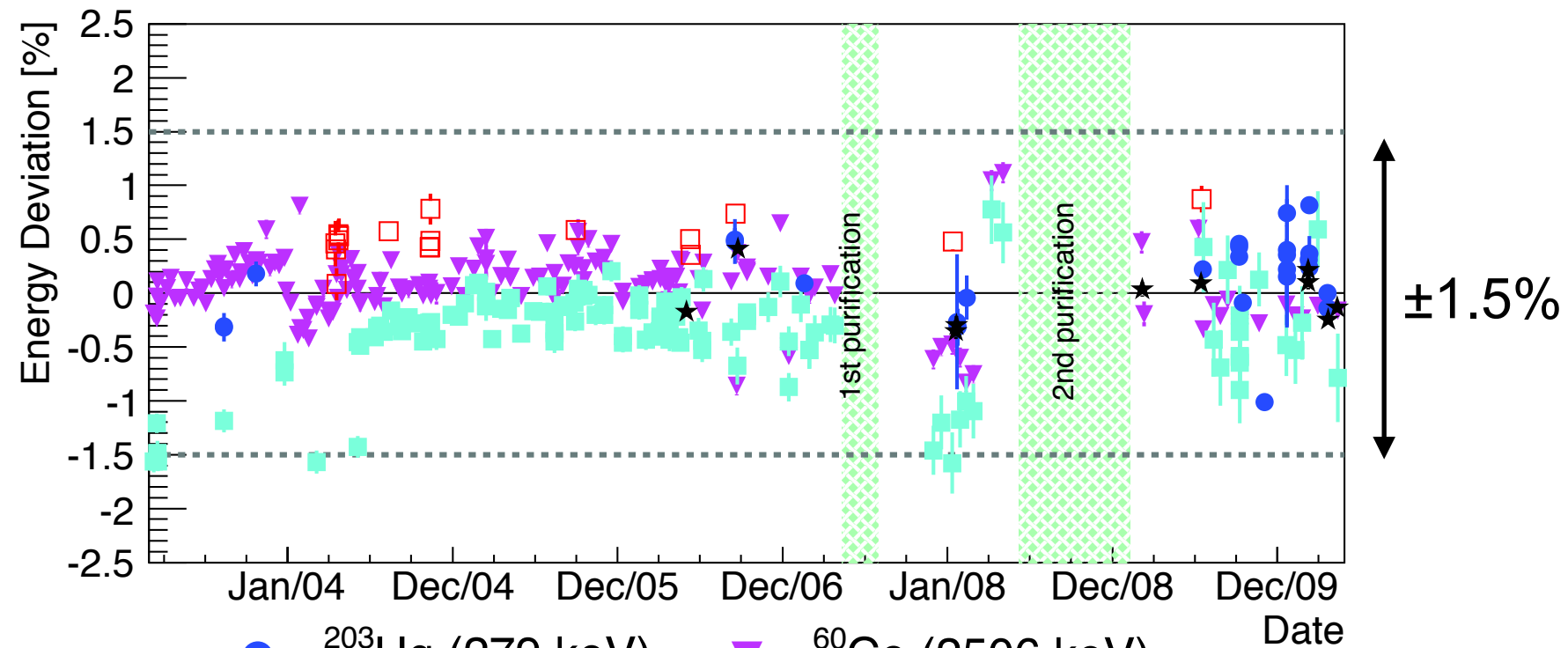
Fig. 8. Activity from a ^{60}Co source deployed to $z = +5, +3, 0, -3, -5$ m along the detector's z -axis, as reconstructed from the data. The colors correspond to the intensity of detected activity. (For interpretation of the references to color in this figure caption, the reader is referred to the web version of this paper.)

Time variation of energy deviation

17 inch

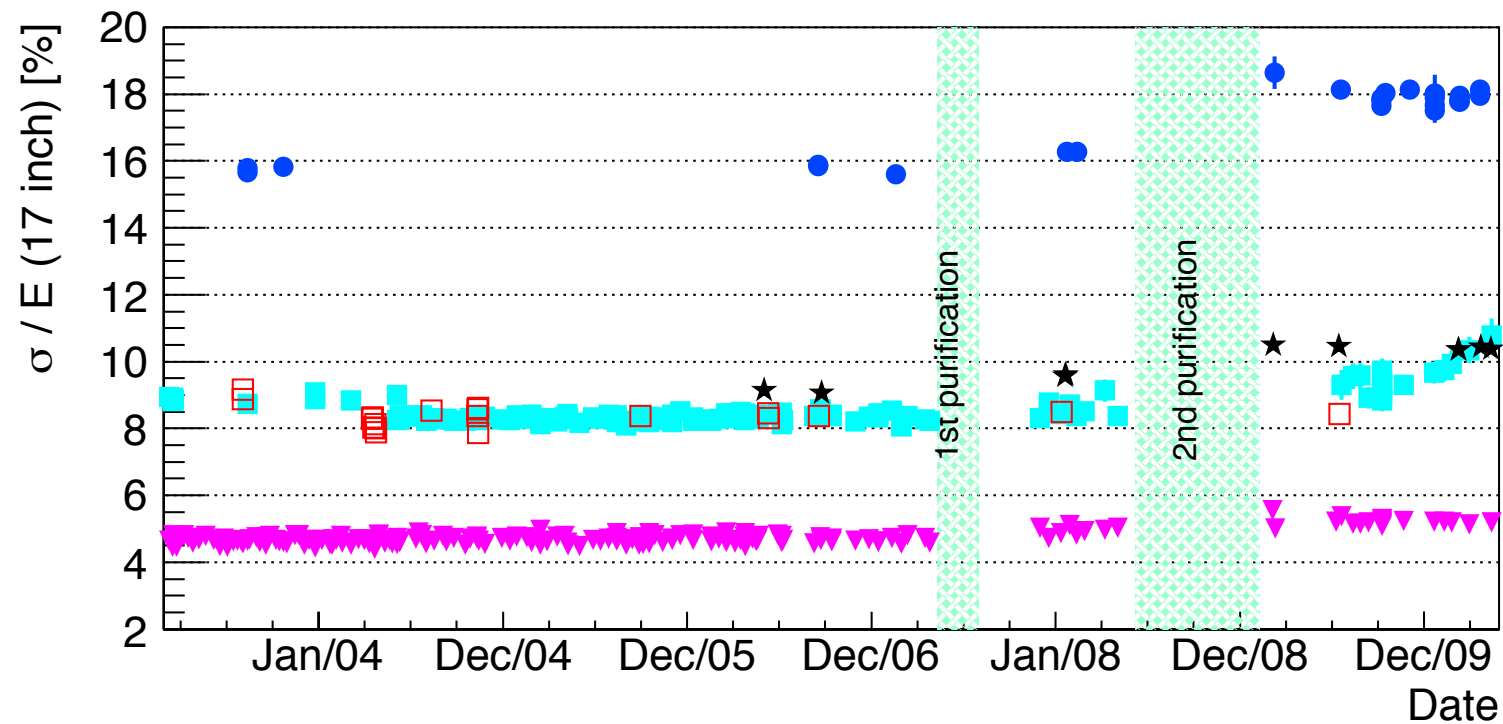


17+20 inch

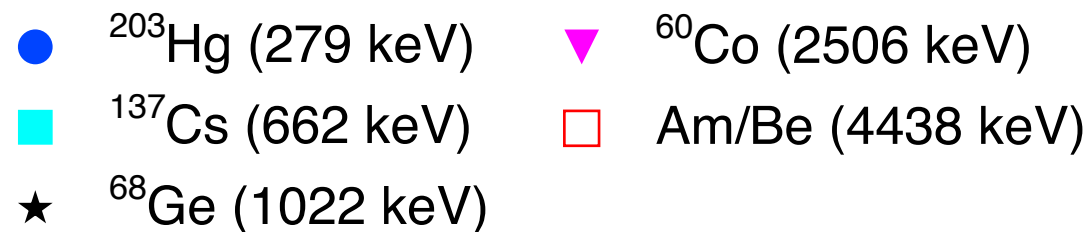
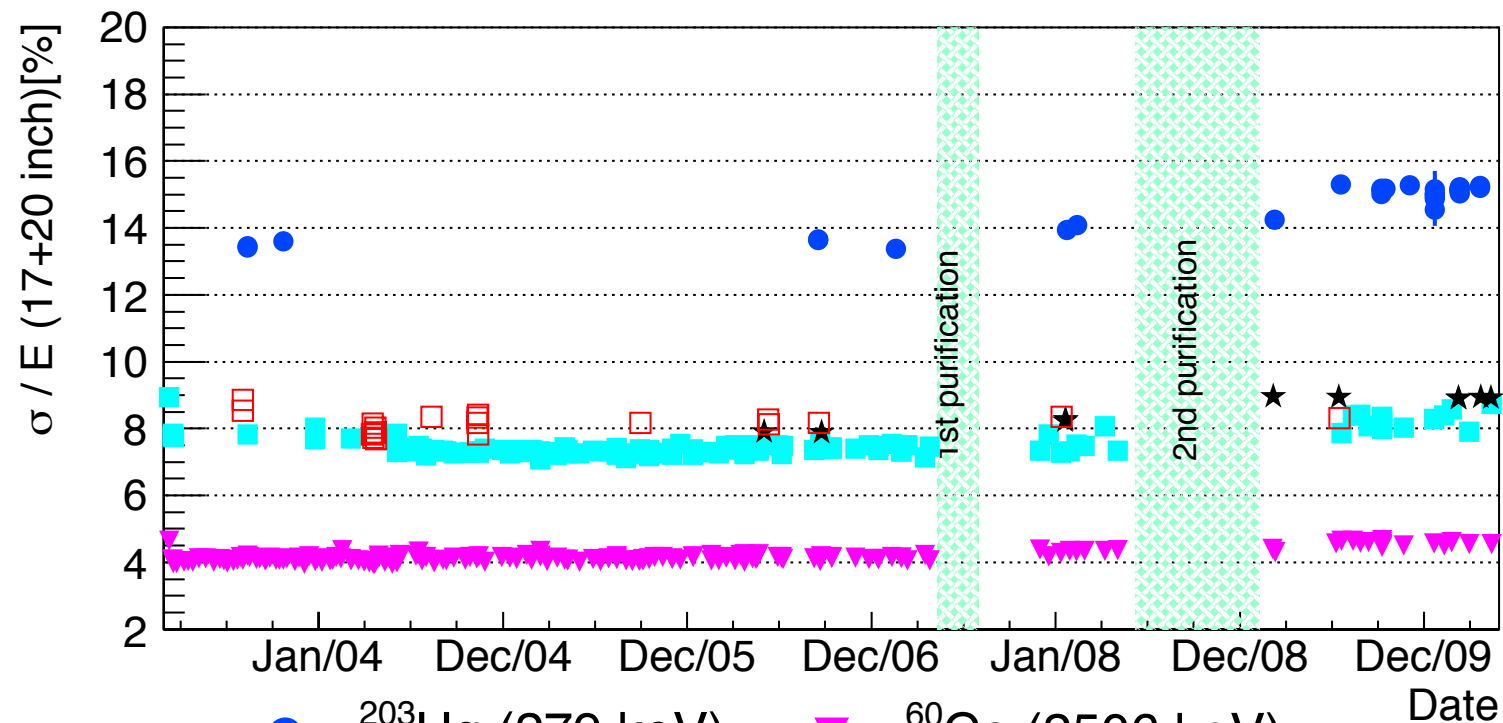


Time variation of energy resolution

17 inch

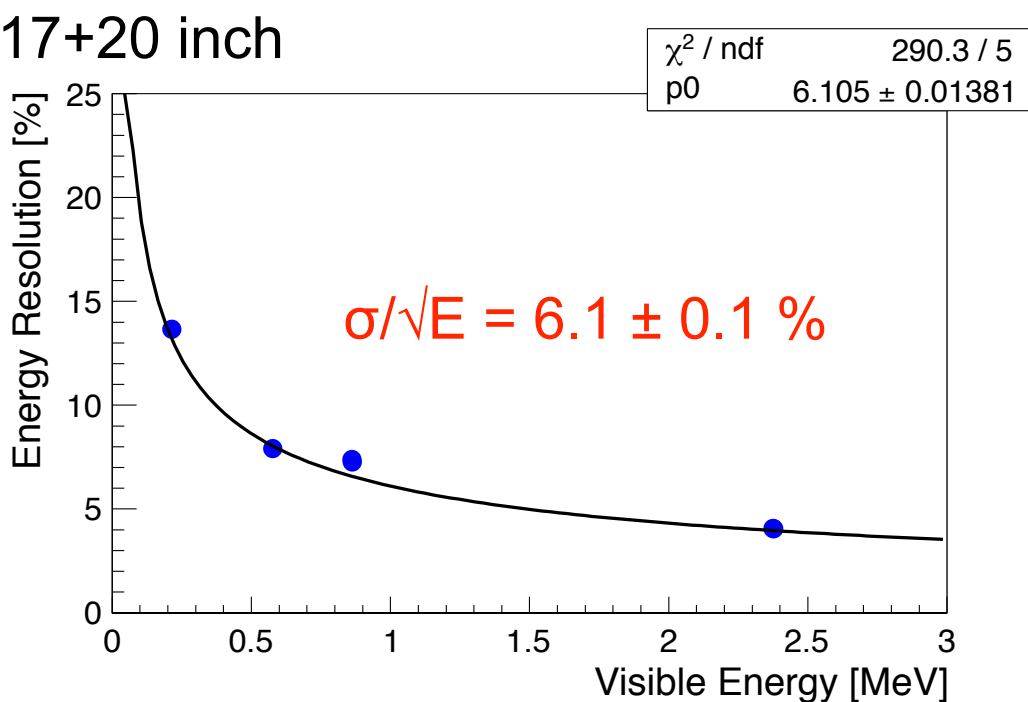
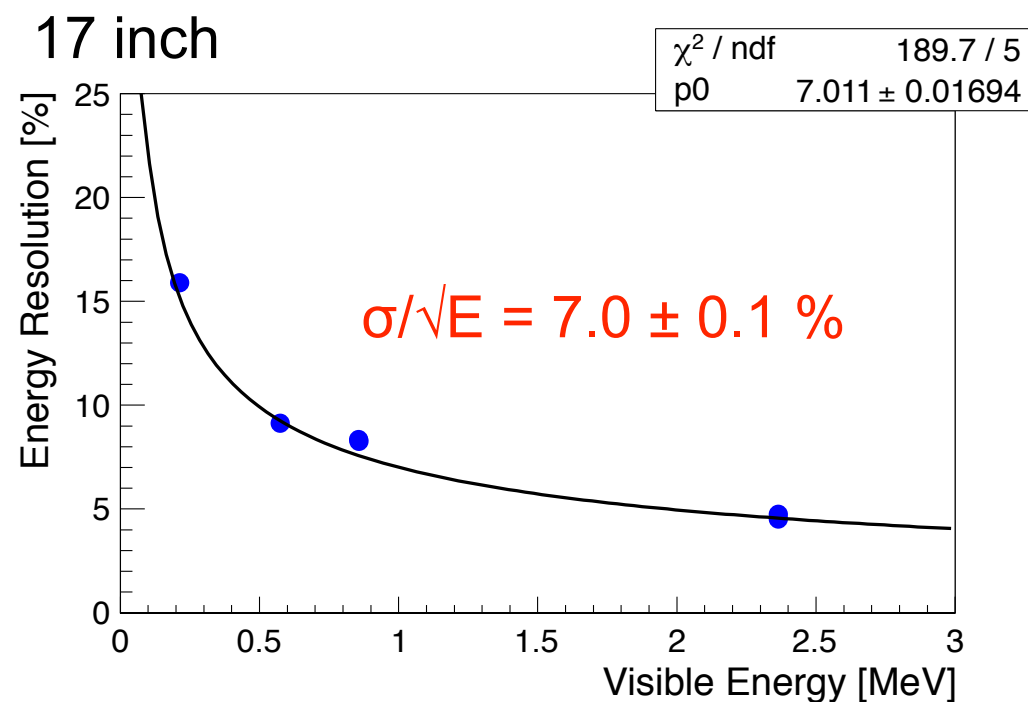


17+20 inch

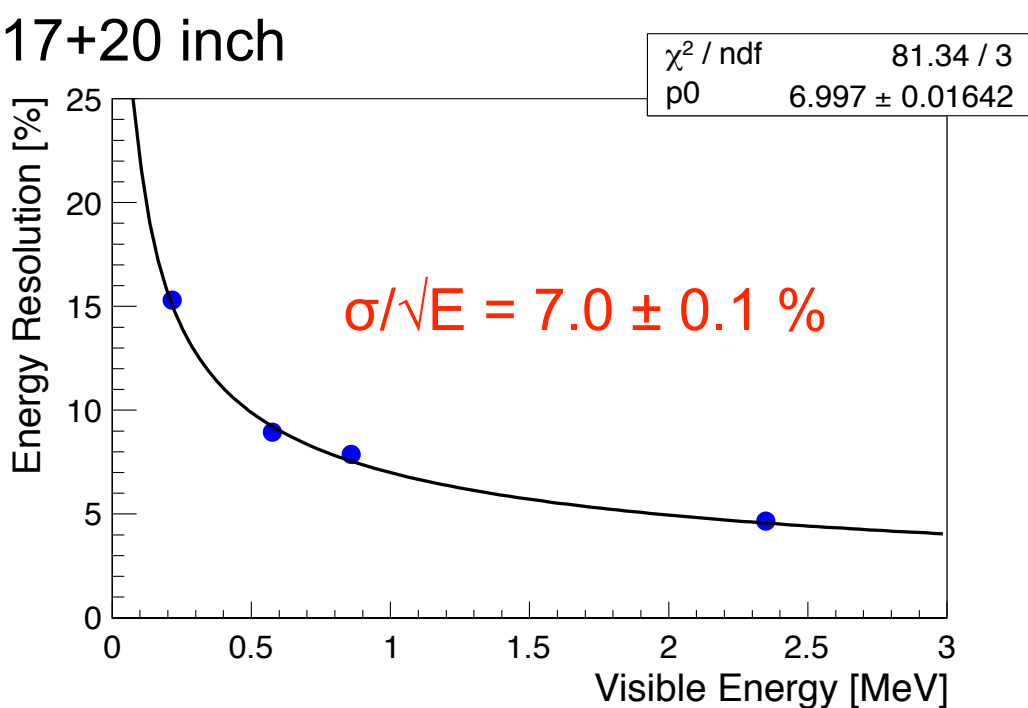
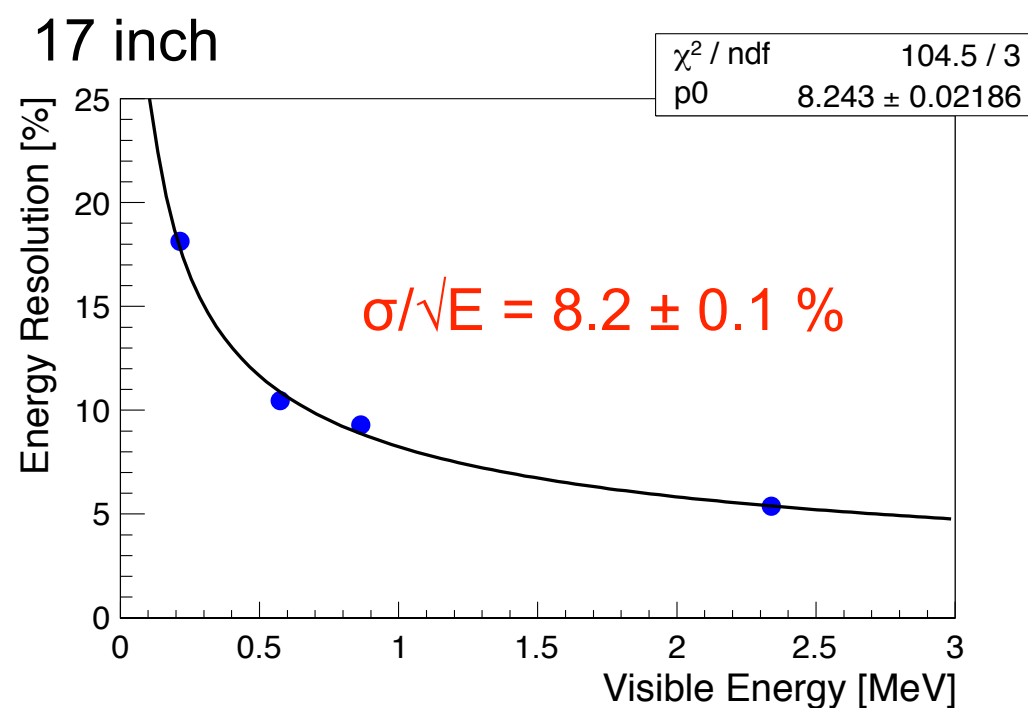


Energy dependent energy resolution

Before Purification

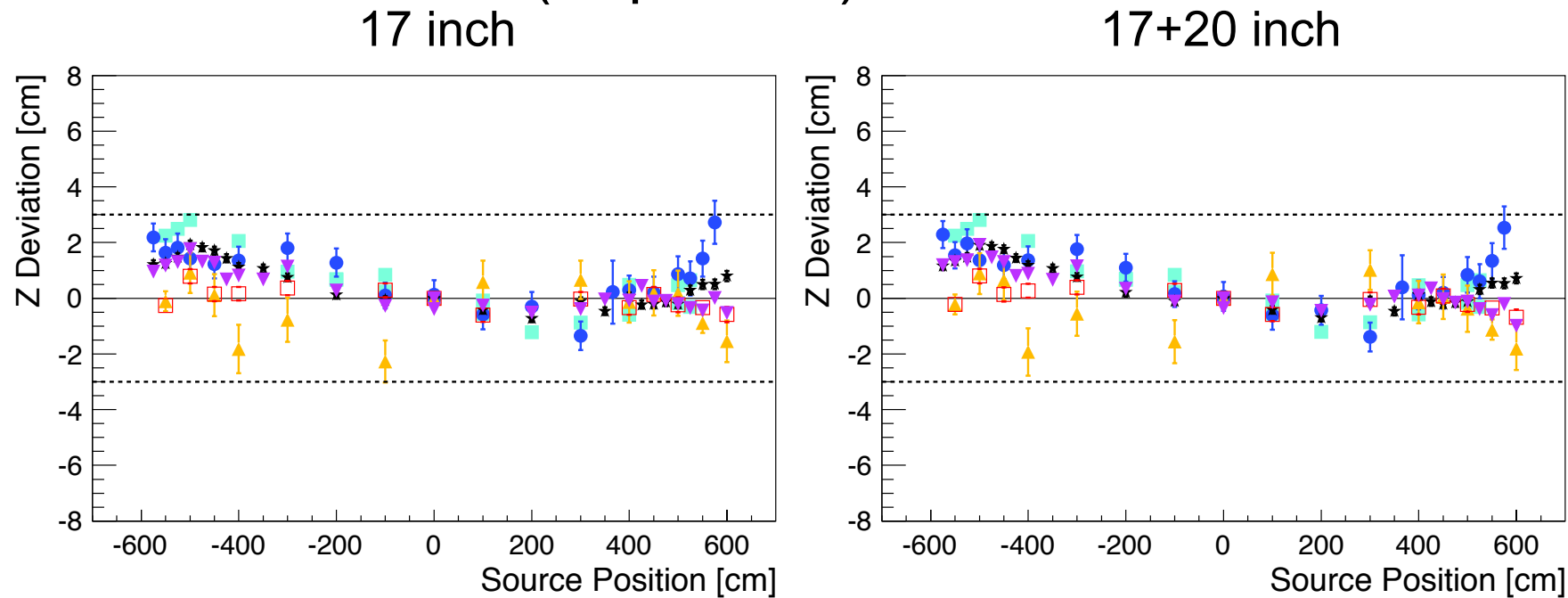


After Purification

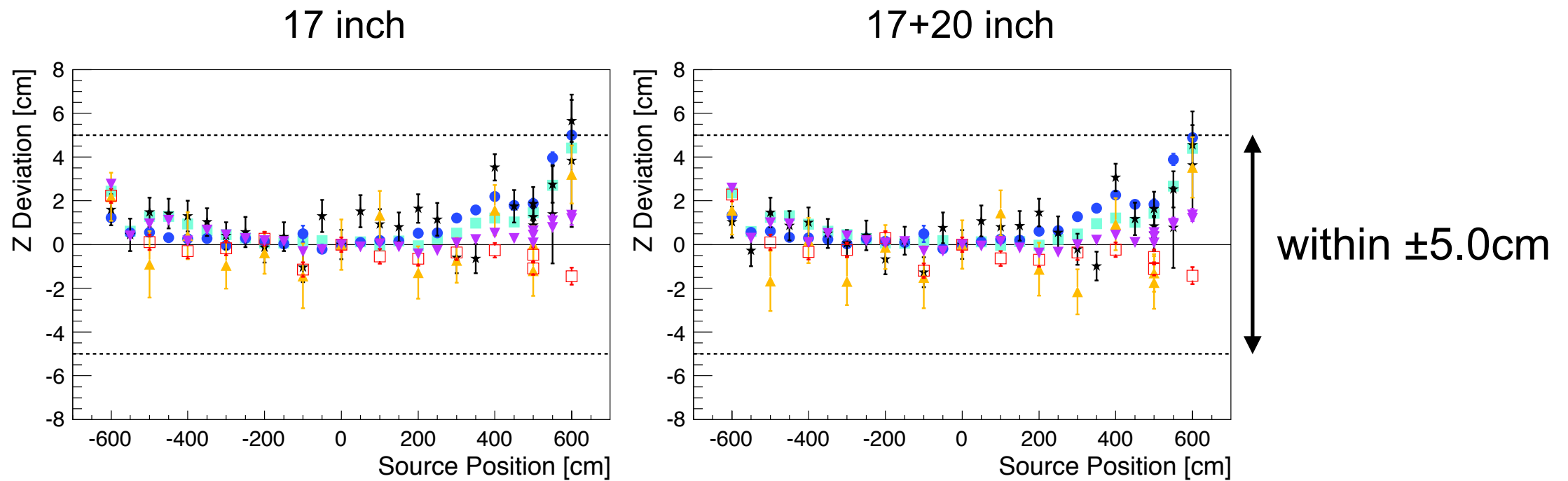


Vertex deviation | z-axis calibration

Before Purification (Sep. 2005)



After Purification (Jul. 2009)



● ^{203}Hg (279 keV)

■ ^{137}Cs (662 keV)

★ ^{68}Ge (1022 keV)

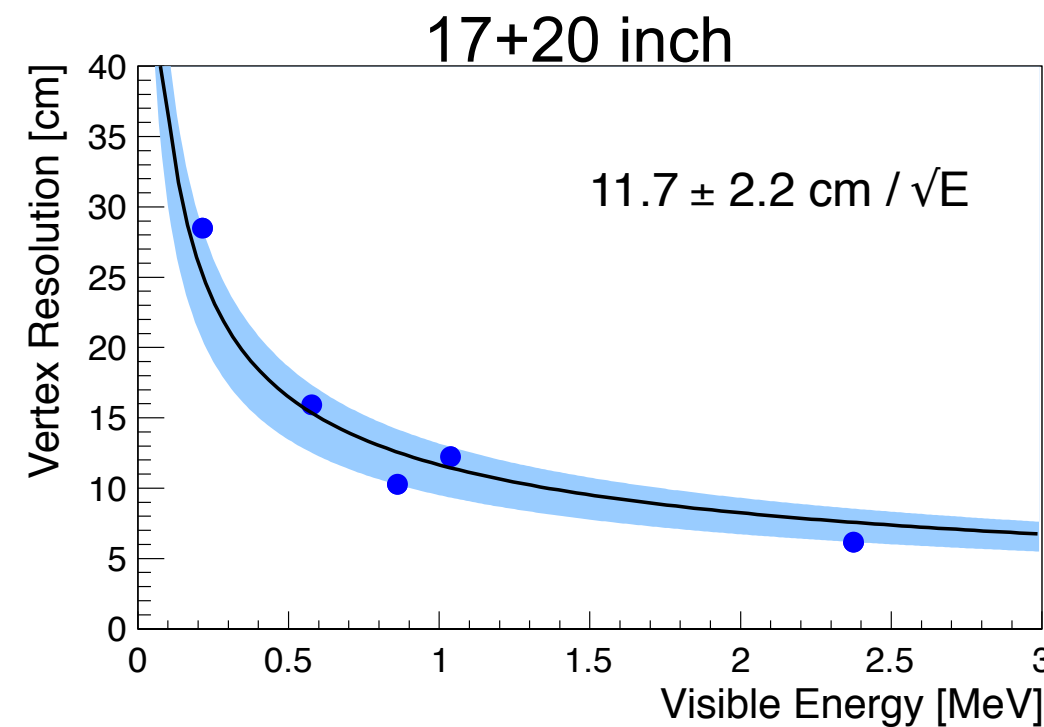
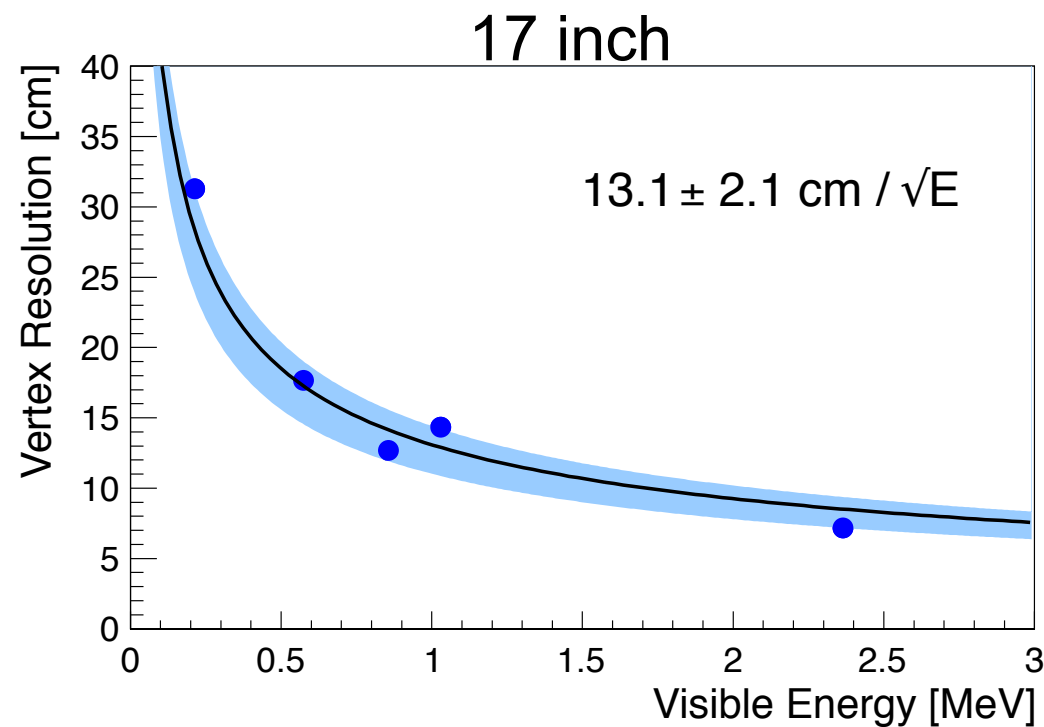
▼ ^{60}Co (2506 keV)

□ Am/Be (4438 keV)

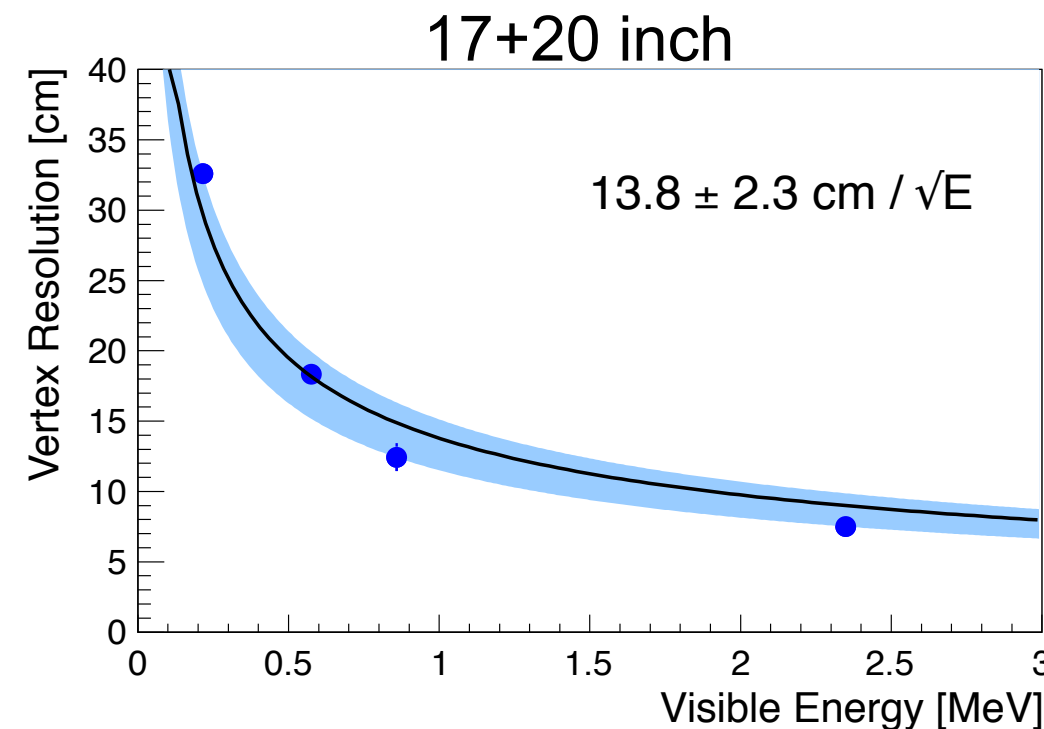
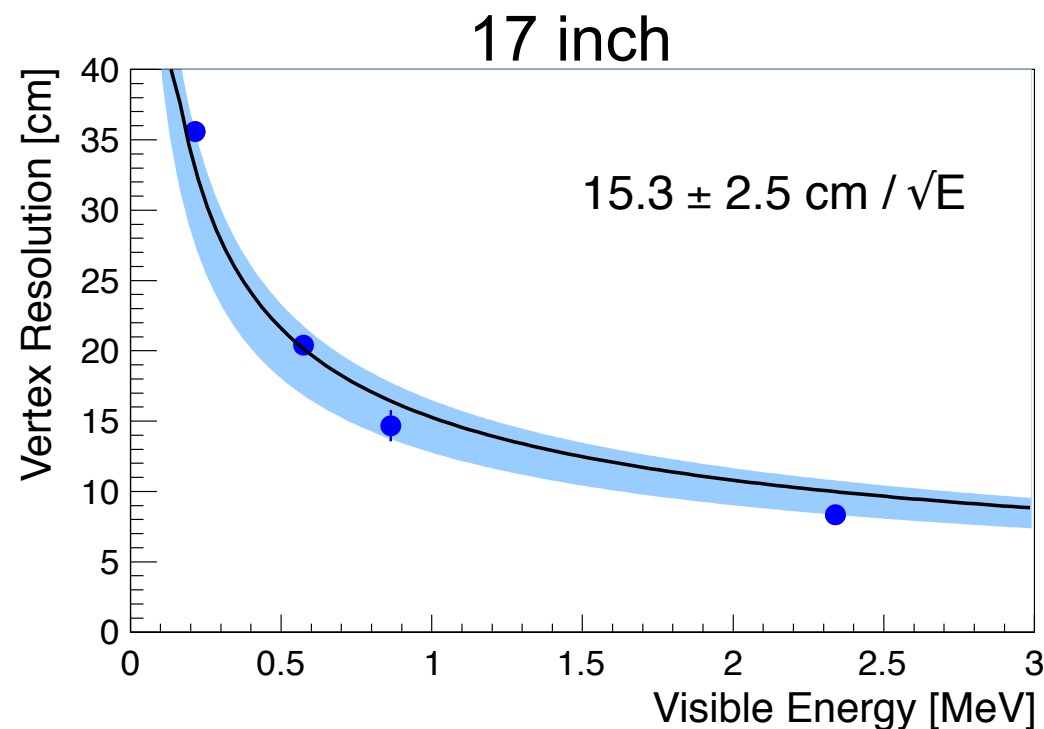
▲ Am/Be (7652 keV)

Energy dependent vertex resolution

Before Purification



After Purification



Neutron capture gamma | Time variation

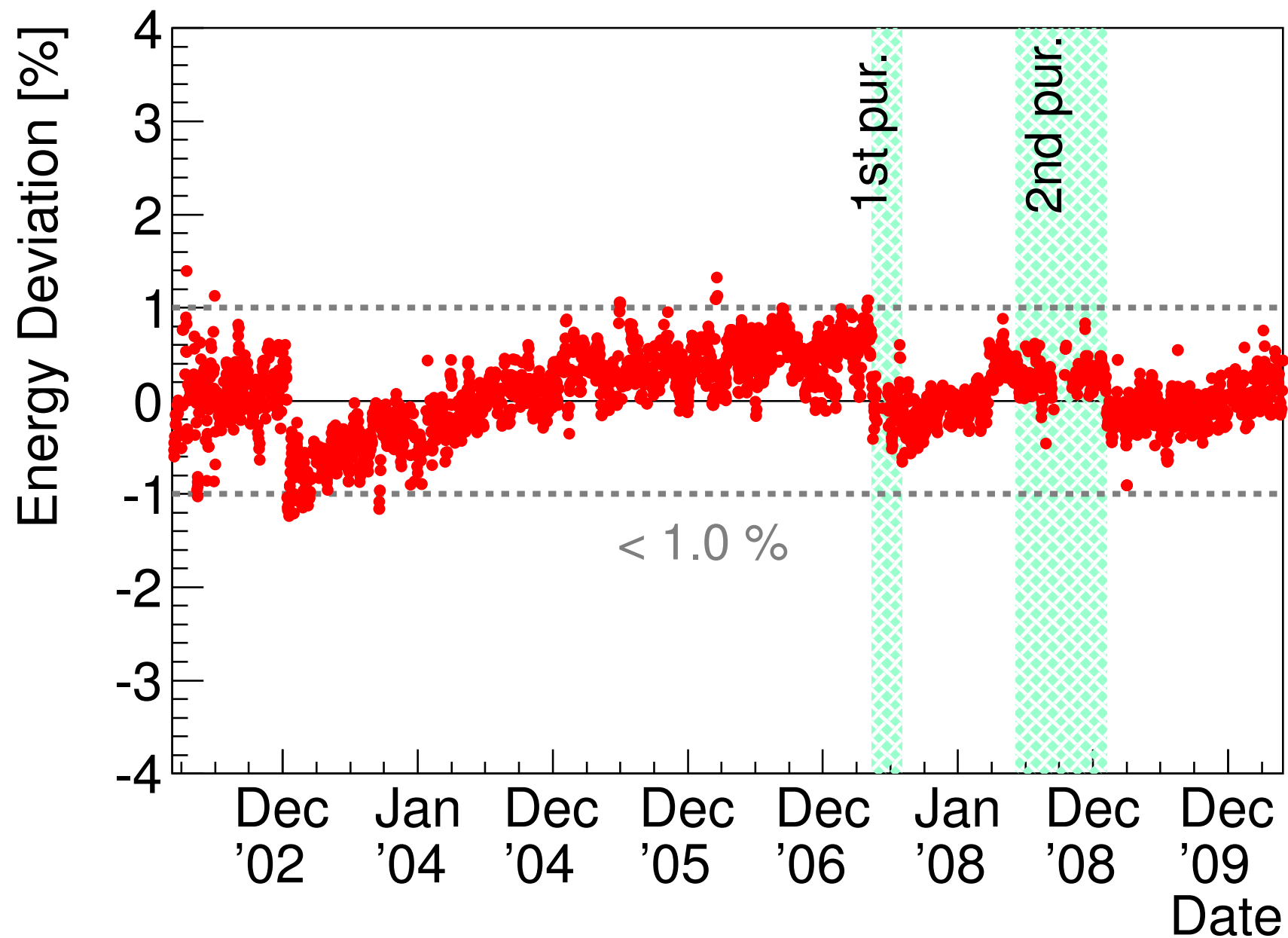
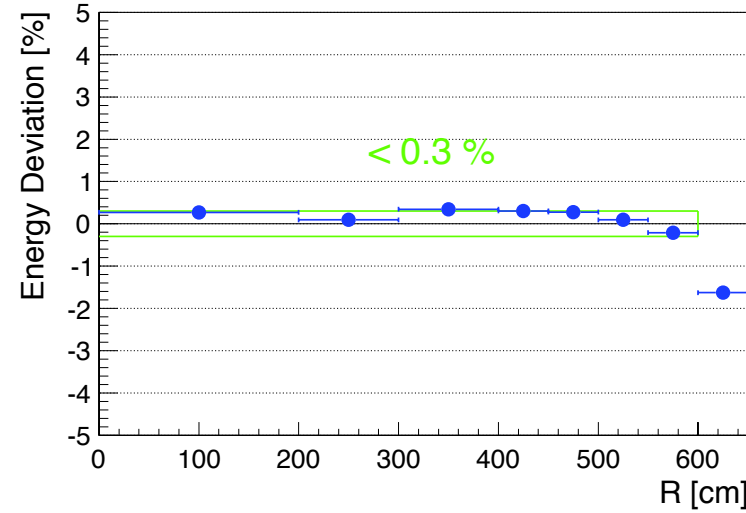


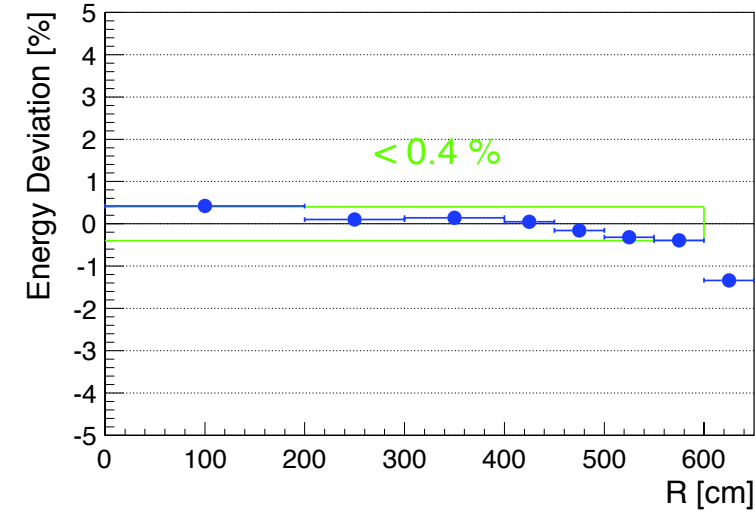
Figure 3.40: Time variation of γ -rays from spallation neutron capture on proton (real energy 2.22457 MeV). The vertical axis shows the deviation between the mean energy estimated by the energy spectrum fitting and the typical visible energy (2.211 MeV). The deviation has been suppressed within ± 1.0 % for all of dataset.

Neutron capture gamma | R&Z dependence

Before Purification



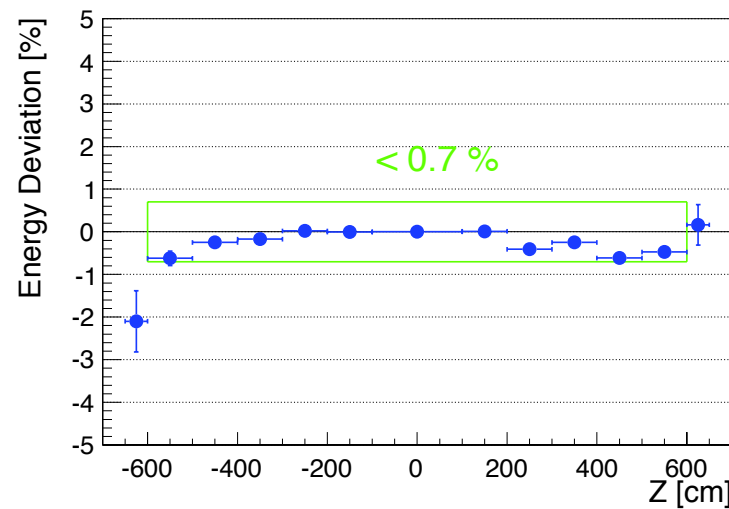
After Purification



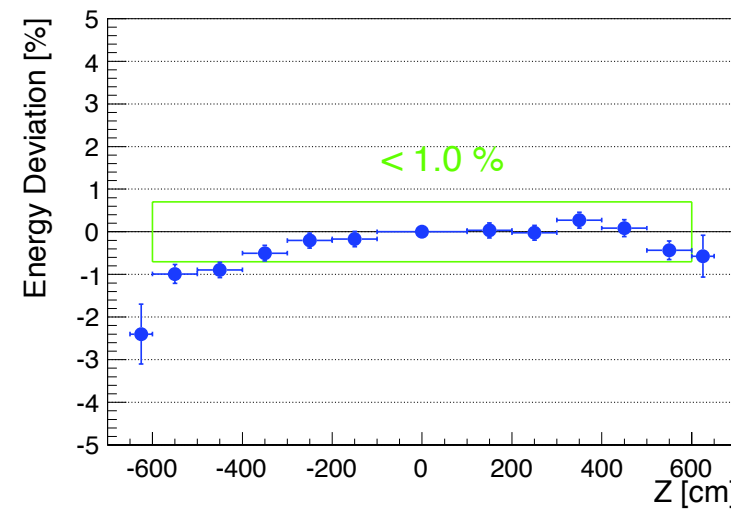
R dependence

Figure 3.41: R dependence of γ -rays from spallation neutron capture on proton before (left) and after (right) purification. The events are selected with $\sqrt{X^2 + Y^2} > 200$ cm. The deviation for before and after purification are estimated to be 0.3 % and 0.4 % in the 6.0 m fiducial radius, respectively.

Before Purification



After Purification



Z dependence

Figure 3.42: R dependence of γ -rays from spallation neutron capture on proton before (left) and after (right) purification. The events are selected with $\sqrt{X^2 + Y^2} < 200$ cm. The deviation for before and after purification are estimated to be 0.7 % and 1.0 % in the 6.0 m fiducial radius, respectively.

Quenching effect

$$\frac{dL}{dx} = L_0 \frac{dE/dx}{1 + k_0 dE/dx}$$

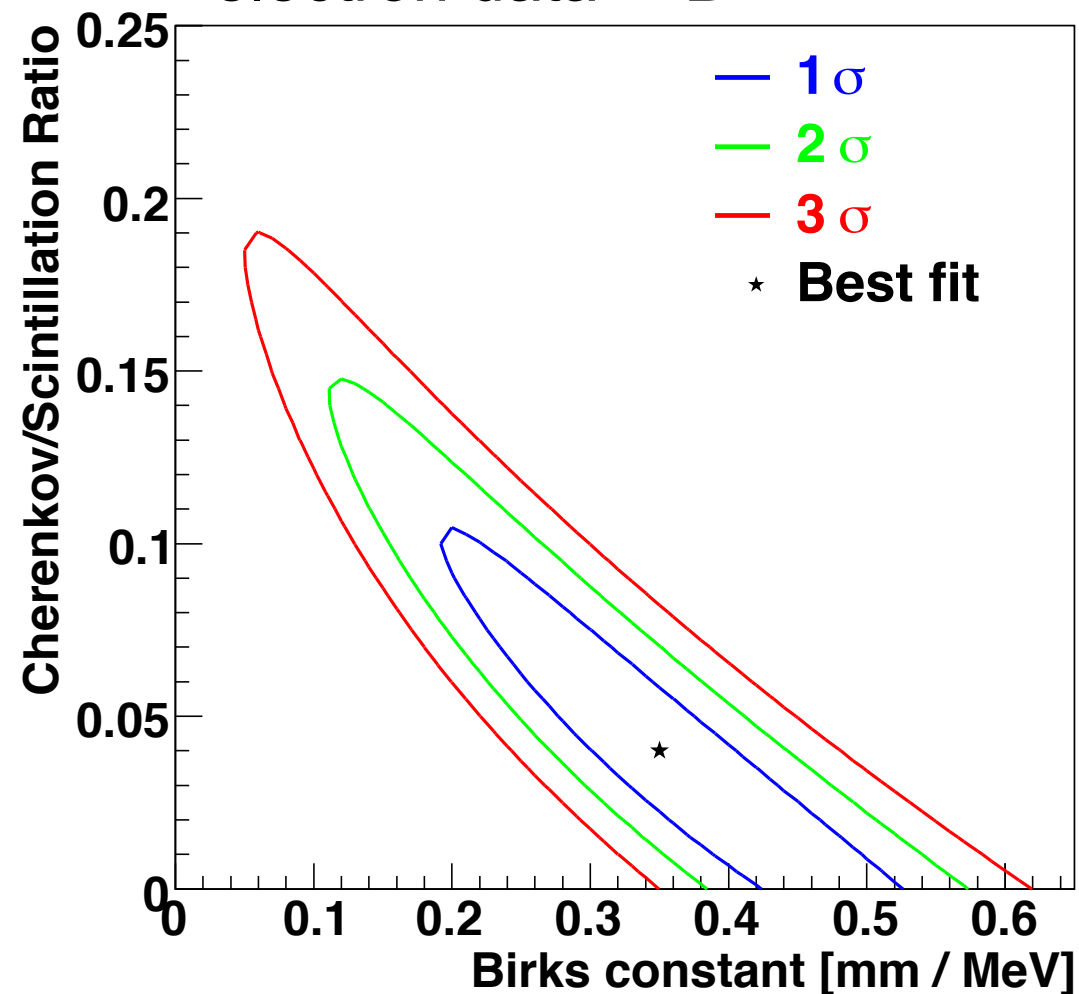
k_0 : Birks constant, L : the luminescence,

L_0 : the luminescence at low specific ionization density and

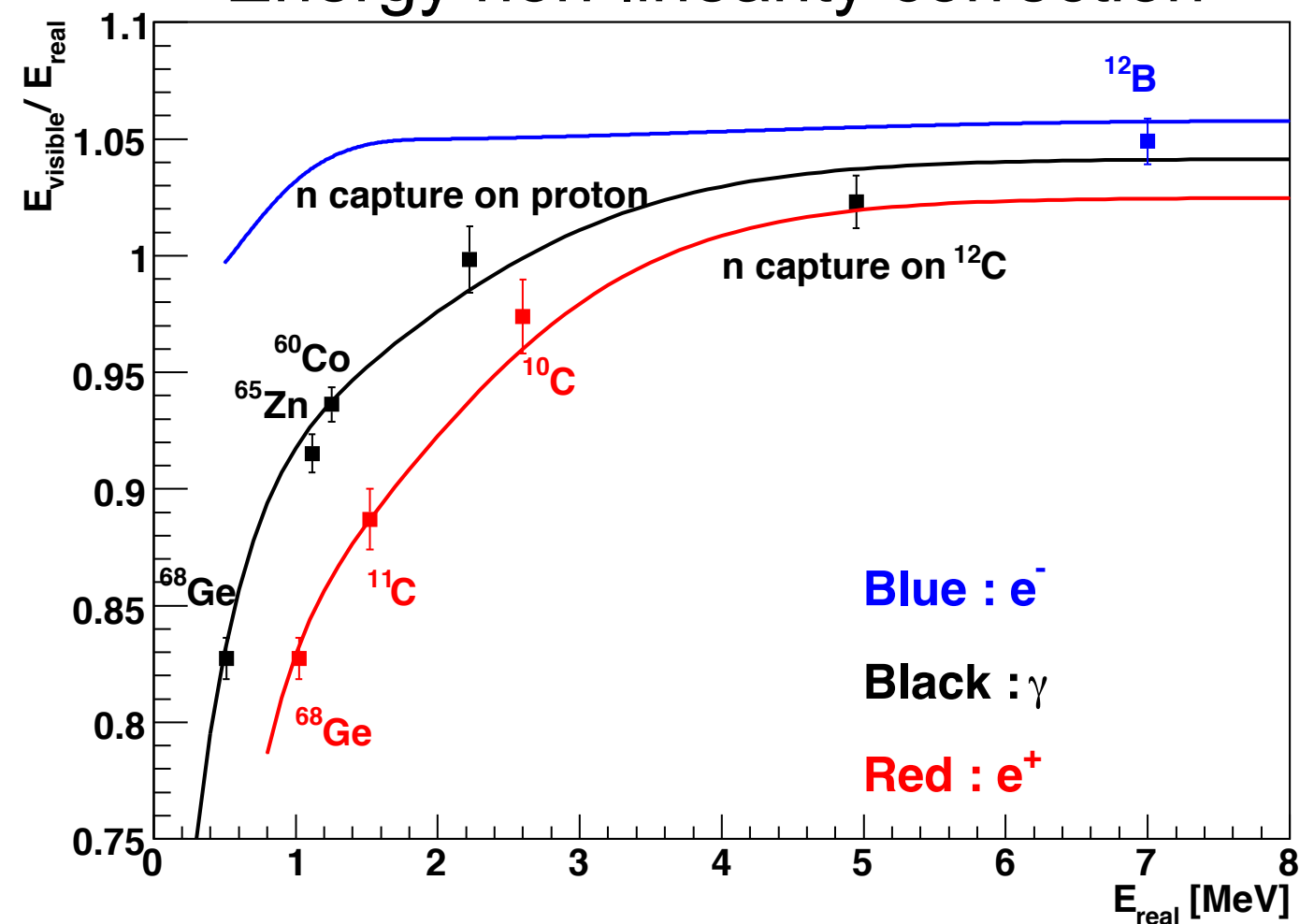
dx/dL : the emitted light intensity per unit length.

Determined by

- 5 gamma ray data (^{60}Co , ^{68}Ge , ^{65}Zn , np, n ^{12}C)
- positron data ^{10}C , ^{11}C ,
- electron data ^{12}B



Energy non-linearity correction



The data points are calibration points.

Summary

KamLAND: 1,000 ton LS
Reactor anti neutrino
Flux-weighted average ~ 180 km

measurement of Δm^2_{21} , $\tan^2\theta_{12}$

No statistical power to measure 5 MeV bump

Systematic uncertainty is dominated by energy scale uncertainty

Source (4pi, z-axis), neutron capture gamma and spallation products are used for energy calibration and energy scale estimation